CHARACTERIZATION OF MECHANICAL PROPERTIES AND STUDY OF MICROSTRUCTURES OF FRICTION STIR WELDED JOINTS FABRICATED FROM SIMILAR AND DISSIMILAR ALLOYS OF ALUMINUM

A Thesis Presented

to the Faculty of the Graduate School

University Of Missouri – Columbia

In Partial Fulfillment

of the Requirements for the Degree

Master of Science

---

by

DEEPA REDDY AKULA

DR. SHERIF EL-GIZAWY, THESIS SUPERVISOR

DECEMBER 2007

The undersigned, appointed by the dean of the Graduate School, have examined the thesis entitled.

CHARACTERIZATION OF PROPERTIES OF FRICTION STIR WELDED JOINTS FABRICATED FROM SIMILAR AND DISSIMILAR ALLOYS OF ALUMINUM

Presented by Deepa Reddy Akula

A candidate for the degree of Master of Science

And hereby certify that in their opinion it is worthy of acceptance.

Dr. Sherif El-Gizawy, Professor, Dept. of Mechanical and Aerospace Engineering

---

Dr. Hao Li, Asst. Professor, Dept. of Mechanical and Aerospace Engineering

---

Luis G. Occeña, Asst. Professor, Dept. Industrial and Manufacturing Systems Engg.

I would like to dedicate all my work and achievements to my father A. Ananda Reddy and my mother A. Vijayananda Reddy for their constant support and encouragement.

ACKNOWLEDGEMENTS

First I would like to thank University of Missouri-Columbia for giving me an opportunity to do the Masters program and for providing me with all the equipment and machinery to carry out the research successfully.

I am grateful to Dr. Serif El-Gizawy, my academic advisor, without his support, and guidance my thesis wouldn't have been successful.

I would like to thank Dr. Hao Li and Dr. Luis Occena for being a member on my thesis committee.

I am thankful for the support I received from the student supervisors of the machine shop Rex Gish, Brain Samuel and Richard Oberto.

I would like to thank my Mother, Father, brothers and friends for being very supportive and encouraging me to achieve my goals.

TABLE OF CONTENTS

LIST OF ILLUSTRATIONS

LIST OF TABLES

CHAPTER 1: INTRODUCTION

1.1 INTRODUCTION OF THE FSW TECHNIQUE

In today's modern world there are many different welding techniques to join metals. They range from the conventional oxyacetylene torch welding to laser welding. The two general categories in which all the types of welding can be divided is fusion welding and solid state welding.

The fusion welding process involves chemical bonding of the metal in the molten stage and may need a filler material such as a consumable electrode or a spool of wire of the filler material, the process may also need a inert ambience in order to avoid oxidation of the molten metal, this could be achieved by a flux material or a inert gas shield in the weld zone, there could be need for adequate surface preparations, examples of fusion welding are metal inert gas welding (MIG), tungsten inert gas welding (TIG) and laser welding. There are many disadvantages in the welding techniques where the metal is heated to its melting temperatures and let it solidify to form the joint. The melting and solidification causes the mechanical properties of the weld to deteriorate such as low tensile strength, fatigue strength and ductility. The disadvantages also include porosity, oxidation, microsegregation, hot cracking and other microstructural defects in the joint. The process also limits the combination of the

metals that can be joined because of the different thermal coefficients of conductivity and expansion of different metals.

The solid state welding is the process where coalescence is produced at temperatures below the melting temperatures of the base metal with out any need for the filler material or any inert ambience because the metal does not reach its melting temperature for the oxidation to occur, examples of solid state welding are friction welding, explosion welding, forge welding, hot pressure welding and ultrasonic welding. The three important parameters time, temperature and pressure individually or in combinations produce the joint in the base metal. As the metal in solid state welding does not reach its melting temperatures so there are fewer defects caused due to the melting and solidification of the metal. In solid state welding the metals being joined retain their original properties as melting does not occur in the joint and the heat affected zone (HAZ) is also very small compared to fusion welding techniques where most of the deterioration of the strengths and ductility begins. Dissimilar metals can be joined with ease as the thermal expansion coefficients and the thermal conductivity coefficients are less important as compared to fusion welding.

Friction stir welding (FSW) is an upgraded version of friction welding. The conventional friction welding is done by moving the parts to be joined relative to each other along a common interface also applying compressive forces across the joint. The frictional heat generated at the interface due to rubbing softens the metal and the soft metal gets extruded due to the compressive forces and the joint forms in the clear material, the relative motion is stopped and compressive forces are increased to form a sound weld before the weld is allowed to cool.

Friction stir welding is also a solid state welding processes; this remarkable upgradation of friction welding was invented in 1991 in The Welding Institute (TWI) [4]. The process starts with clamping the plates to be welded to a backing plate so that the plates do not fly away during the welding process. A rotating wear resistant tool is plunged on the interface between the plates to a predetermined depth and moves forward in the interface between the plates to form the weld. The advantages of FSW technique is that it is environment friendly, energy efficient, there is no necessity for gas shielding for welding Al, mechanical properties as proven by fatigue, tensile tests are excellent, there is no fume, no porosity, no spatter and low shrinkage of the metal due to welding in the solid state of the metal and an excellent way of joining dissimilar and previously unweldable metals.

1.2 BRIEF HISTORY OF FRICTION WELDING

Friction welding is a solid state welding where two metals are joined without any filler material, heating source and inert environment. Friction welding can be broadly divided into three categories rotary welding, non-rotary welding and friction processing.

The friction welding technologies convert the mechanical energy into material deformation and heat energy to create a weld. Rotary welding was the first of all the different friction welding processes to be developed and used commercially. In this welding process, one cylindrical shaped object which has to be joined is rotated against a similar fixed component under predetermined pressure. The material at the faying surface softens due to the friction heat and the parts are subsequently forged together. The rotary welding process can be used to join similar or dissimilar metals. There are two methods of supplying the energy for the rotary friction welding processes which are continuous drive rotary friction welding, and stored energy friction welding or inertial welding.

In continuous drive rotary friction welding process one part is connected to a motor running at a controlled speed. The other part is held stationary. The rotation continues until an axial shortening is reached and an axial force is maintained to complete the weld [2].

In stored energy friction welding or inertia welding, the rotating component is attached to a flywheel which is accelerated to a preset rotation speed. At this point the power drive to the flywheel is cut. The rotating flywheel which has a set amount of stored energy is then forced against the stationary component and the resultant braking action generates the required heat for welding.

Non-rotary welding was another major advance process. Linear, orbital and angular reciprocating motions permit the joining of noncircular shapes such as squares and rectangular bars, which are very difficult to weld with rotary technology to provide correct alignment.

1.3 ALUMINUM ALLOYS AND WELDING OF ALUMINUM ALLOYS

Aluminum is the most abundant metal available in the earths crust, steel was the most used metal in 19th century but Aluminium has become a strong competitor for steel in engineering applications. Aluminium has many attractive properties compared to steel it is economical and versatile to use that is the reason it is used a lot in the aerospace, automobile and other industries. The most attractive properties of aluminum and its alloys which make them suitable for a wide variety of applications are their light weight, appearance, frabricability, strength and corrosion resistance. The most important property of aluminum is its ability to change its properties in a very versatile manner; it is amazing how much the properties can change from the pure aluminum metal to its most complicate alloys. There are more then a couple of hundreds alloys of aluminum alloys and many are being modified form them internationally. Aluminium alloys have very low density compared to steel it has almost one thirds the density of steel. Properly treated alloys of aluminum can resist the oxidation process which steel can not resist; it can also resist corrosion by water, salt and other factors.

There are many different methods available for joining aluminum and its alloys. The selection of the method depends on many factors such as geometry and the material of the parts to be joined, required strength of the joint, permanent or dismountable joint, number of parts to be joined, the aesthetic appeal of the joint and the service conditions such as moisture, temperature, inert atmosphere and corrosion.

Welding is one of the most used methods for aluminum. Most alloys of aluminum are easily weldable. MIG and TIG are the welding processes which are used the most, but there are some problems associated with this welding process like porosity, lack of

fusion due to oxide layers, incomplete penetration, cracks, inclusions and undercut, but they can be joined by other methods such as resistance welding, friction welding, stud welding and laser welding. When welding many physical and chemical changes occur such as oxide formation, dissolution of hydrogen in molten aluminum and lack of color change when heated.

The formation of oxides of aluminum is because of its strong affinity to oxygen, aluminum oxidizes very quickly after it has been exposed to oxygen. Aluminum oxide forms if the metal is joined using fusion welding processes, and aluminum oxide has a high melting point temperature than the metal and its alloys it self so it results in incomplete fusion if present when joined by fusion welding processes. Aluminum oxide is a electrical insulator if it is thick enough it is capable of preventing the arc which starts the welding process, so special methods such as inert gas welding, or use of fluxes is necessary if aluminum has to be welded using the fusion welding processes.

Hydrogen has high solubility in liquid aluminum when the weld pool is at high temperature and the metal is still in liquid state the metal absorbs lots of hydrogen which has very low solubility in the solid state of the metal. The trapped hydrogen can not escape and forms porosity in the weld. All the sources of hydrogen has to be eliminated in order to get sound welds such as lubricants on base metal or the filler material, moisture on the surface of base metal or condensations inside the welding equipment if it uses water cooling and moisture in the shielding inert gases. These precautions require considerable pretreatment of the workpiece to be welded and the welding equipment.

Hot cracking is also a problem of major concern when welding aluminum, it occurs due to the high thermal expansion of aluminum, large change in the volume of the metal

upon melting and solidification and its wide range of solidification temperatures. The heat treatable alloys have greater amounts of alloying elements so the weld crack sensitivity is of concern. The thermal expansion of aluminum is twice that of steel, in fusion welding process the melting and cooling occurs very fast which is the reason for residual stress concentrations.

Weldability of some aluminum alloys is an issue with the fusion welding processes. The 2000 series, 5000 series, 6000 series and 7000 series of aluminum alloys have different weldabilities. The 2000 series of aluminum alloys have poor weldability generally because of the cooper content which causes hot cracking and poor solidification microstructure and porosity in the fusion zone so the fusion welding processes are not very suitable for these alloys. The 5000 series of aluminum alloys with more than 3% of Mg content is susceptible to cracking due to stress concentration in corrosive environments, so high Mg alloys of 5000 series of aluminum should not be exposed to corrosive environments at high temperatures to avoid stress corrosion cracking. All the 6000 series of aluminum are readily weldable but are some times susceptible to hot cracking under certain conditions. The 7000 series of aluminum are both weldable and non-weldable depending on the chemical composition of the alloy. Alloys with low Zn-Mg and Cu content are readily weldable and they have the special ability of recovering the strength lost in the HAZ after some weeks of storage after the weld. Alloys with high Zn-Mg and Cu content have a high tendency to hot crack after welding. All the 7000 series of aluminum have the sensitivity to stress concentration cracking.

All these problems associated with the welding of these different alloys of aluminum has lead to the development of solid state welding processes like Friction Stir Welding technique which is an upgraded version of the friction welding processes. This process

has many advantages associated with it, and it can weld many aluminum alloys such as 2000 and 7000 series which are difficult to weld by fusion welding processes. The advantages of the Friction Stir Welding processes are low distortion even in long welds, no fuse, no porosity, no spatter, low shrinkage, can operate in all positions, very energy efficient and excellent mechanical properties as proven by the fatigue, tension and bend tests.

1.4 FRICTION STIR WELDING AND ITS APPLICATIONS

Friction stir welding process is a new welding technique which joins materials by plasticizing and then eventually consolidating the material around the joint line of the weld. First the base metal pieces which have to be joined are held suitable clamping force so that the work pieces do not fly away while welding. A rotating steel pin pierces a hole in the joint line between the workpieces to a predetermined depth and moves forward in the direction of the weld as shown in Figure-1.

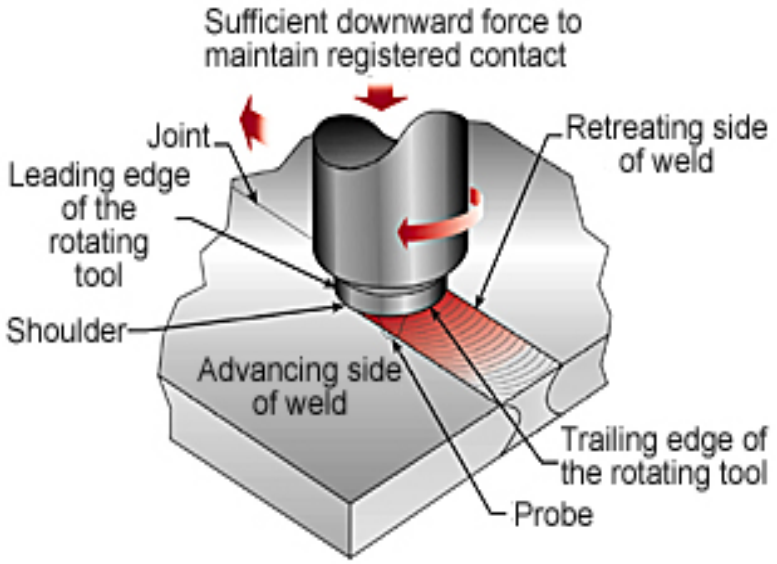

Figure-1 Schematic of Friction Stir Welding process

As the pin moves forward it plasticizes the material due to the frictional heat generated by the rupture between the wear resistant steel pin and the workpiece. The force provided by the pin forces the plasticized material to the rare of the pin. This material cools and then consolidates to form a bond in the solid state of the material.

There is no melting and the weld is in hot worked condition with no much entrapped gases and porosity and the weld nugget has fine grained microstructure.

Friction stir welding is appropriate method for aluminum alloys with Cu, Mg and Si content as it does not involve melting which creates problems like hot cracking, porosity and solidification shrinkage in certain alloys. It does not need shielding gas which is commonly required for other processes to protect the molten weld pool. It is mostly insensitive to contaminations so, oxide removal immediately prior to weld or other cleaning procedures which are a must for arc welding are not necessary. The friction stir welding process is not limited to any one position and is feasible to operate in any position as there is no formation of molten metal weld pools involved while welding. The process is simple and does not need highly skilled operator which is a compulsion for other arc welding processes. The operator could run sound welds with minimal training. Many complicated shapes can be fabricated by the friction stir welding processes these shapes could be very difficult and costly if considered casting or extrusion processes for fabrication. The process is clean does not have any major safety hazards like poisonous fumes or harmful radiations, so it can be conducted in any ambience with out much preparation which are a must for arc welding processes. Many companies have already started switching from gas metal arc welding process to friction stir welding process. Many companies in aerospace industry have adopted friction stir welding because it is cost and energy efficient.

Some of the attractive features which are forcing manufacturing firms to adopt friction stir welding are non consumable tool, one tool can typically used for 1000m of weld length in 6000 series aluminum, no filler wire required, no gas shielding for welding aluminum, no welder certification required, no need for work piece preparations as small

oxide layers are accepted, no need for grinding, brushing or pickling is required in mass production.

There are some disadvantages associated with this welding process the welding speed could be very slow for single pass welding techniques, the workpiece should be clamped very well with high clamping force in order to avoid accidents when the tool is plunged in between the plates to be welded and at the end of each weld there is a hole due to withdrawal of the pin from the plates. The hole due to the pin is filled by other welding processes in many cases for aesthetic purposes.

1.5 LITERATURE REVIEW

Friction stir welding (FSW) is a new welding process that has produced low cost and high quality [10] joints of heat-treatable aluminum alloys such as AA 2024 and AA7075 without introducing a cast microstructure [4], alloys of aluminum belonging to the 2000 series have limited weldability and the 7000 series are generally not recommended for welding as a joining method. The welding of aluminum and its alloys has always represented a great challenge for researchers and technologists. There are lots of difficulties associated with the friction stir welding process, mainly due to the presence of a tenacious oxide layer, high thermal conductivity, high coefficient of thermal expansion, solidification shrinkage and high solubility of hydrogen in molten state [14].

Friction Stir Welding (FSW) is becoming the choice of the industry for structurally demanding applications. FSW process does not cause severe distortion and residual stresses as compared to the traditional welding processes [17]. This result is fortified by other authors also who observed that severe distortions and the generated residual stresses are very low in Friction stir welding process compared to the traditional welding processes as concluded by P.Cavaliere and R.Nobile [6]. Heat-treatable aluminum alloys of 2XXX and 7XXX series are difficult to join by the fusion welding because of induced defects such as crack and porosity can form easily in the weld during the solidification of the molten metal as gases such as hydrogen are highly soluble in the weld tool. Further problems arise when attention is focused on heat-treatable alloys as heat provided by welding process, is responsible of the

decay of mechanical properties, due to phase transformations and softening induced in alloy.

Friction-stir welding of aluminum alloys has been employed in many industries to improve the quality of the resulting joint [5]. Industries are approaching the friction stir welding process to face automotive and aerospace structural joining difficulties as FSW. The production of welded aluminum structural sheets with high, reliable tensile and fatigue properties are very important in commercial and military applications. Joining technologies for the 2XXX and 7XXX aluminum sheet alloys is important as it directly affects the material choice for the future modern aircraft and automobile, so P.Cavaliere and R.Nobile recognized the need to implement advanced joining technologies [6].The application fields of FSW are marine (hulls, superstructures, decks, and internal structures for high speed ferries and LPG storage vessels for the shipbuilding industry), aerospace (Airframes, fuselages, wings, fuel tanks), railway (high speed trains, railway wagon and coachwork, and bulk carrier tanks), automotive (chassis, wheel rims, space frames, truck bodies), motorcycle, electrical and refrigeration industries.

Experimental Investigation of effects of Tungsten inert gas (TIG) and Friction stir welding (FSW) on microstructure and corrosion resistance of AA 2024-T3 welded butt joints was carried out by A. Squillace [17]. The study of micro hardness measurements shows a general decay of mechanical properties of TIG joints which is due to high temperatures experienced by material during the welding process. Friction-stir welding process joins the metal by stirring of one metal work piece into another which induces extreme plastic deformation [7]. For FSW joints the author found that the joints have experienced lower temperatures and severe plastic deformations than the TIG induced by tool motion allowing the rise of a complex

thermo-mechanical situation. It was observed that there was a slight decay of mechanical properties in the nugget zone, flow arm and thermo-mechanically altered zone (TMAZ) on the other hand in the heat-affected zone (HAZ) a light improvement of mechanical properties was observed. In flow arm and in nugget zone a slight recovery of hardness, with respect to the TMAZ zone was recorded due to the re-crystallization and formation of a very fine grain structure [14]. Mechanical properties of FSW joints are quite good and fatigue properties are practically the same as the parent metal. The tensile failures generally occur well away from the nugget.

Research on the microstructural characteristics and mechanical properties of the friction-stir-welded joints by H.J.Liu and H.Fujii have concluded that FSW softens the joints of the heat-treatable aluminum alloys such as 2024-T3 and 7075-T6 because the strengthening precipitates dissolve and grows during the welding thermal cycle which results in the degradation of the mechanical properties of the joints [10].

Study of the micro structures of friction-stir welded joints by Michael A. Sutton, Bangcheng Yang suggests that the FSW process introduces a well defined variation in grain size between different zones within the process zone [5]. P.Cavaliere and R.Nobile [6] concluded that "the higher temperatures and severe plastic deformations result in remarkable smaller grains compared to the base metal" [6]. Research done by M. Cabibbo, H.J. McQueen E. Evangelista [8] reinforce the fact that fine worked and recrystallized grain structure is formed by stirring and forging of the parent alloy [8]. On a typical transverse cross-section of the friction stir welded zone, a highly refined grains and equiaxial grain structure is found in the nugget zone, with a very distinctive transition in grain size on the advancing side and

a gentle transition in grain size was recorded on the retreating side. The smallest grain size was generally observed on the top surface of the weld nugget where contact occurs with the tool shoulder [5].According to the study of William D. Lockwood, Borislav Tomaz [9] the transitions from the TMAZ to the HAZ and from the HAZ to the base material are gradual and not distinguished by any sharp change in microstructure [9]. The study by C.G. Rhodes, M.W. Mahoney, and W.H. Bingel has considered the microstructural changes of Al 7075 only at travel speed of 5 in/min and did not specify the reason for using 5 in/min as the travel speed for the weld [4]. A study of micro structures by M. Cabibbo, H.J. McQueen E. Evangelista concluded that the retreating side is wider due to tool rotation causing the material ahead of it to move to the right hand side and the advancing side is narrower. They also observed that the "strain rate and temperature gradients are much steeper in the advancing side than in the retreating" [8].

Well defined micro structural bands are the micro structural feature generally observed in FSW nugget region was the focus of the research of Michael A. Sutton, Bangcheng Yang [5]. They concluded that the onion ring banded structure is because of the nominal cylinders of the metal being extruded by the tool and shredding these sheets of metal during the rotation of the tool. The bands of distinctive hardness maxima and minima have been observed in the HAZ. Though the authors have not investigated they predict that these bands are due to the presence of the onion rings. Investigations performed by P. Cavaliere, E. Cerri and A. Squillace [17] on the transverse cross-sections of the specimens of the FSW process of the 2024 and 7075 aluminum alloys revealed the formation of the elliptical "onion" structure in the centre of the weld [17].

Research on the tensile properties and fracture locations by by H.J.Liu and H.Fujii [10] reveal that if a friction stir welded joint is free of micro and macro defects, the tensile properties of the tailored joint is only dependent on the micro hardness distributions across the joint. The presence of regions such as the weld nugget, two TMAZs and two HAZs are the hardness degradation regions in the joint which are indicated to lower the tensile properties of the joints than those of the base material [10].

P. Cavaliere, E. Cerri and A. Squillace [17] have studied the mechanical and microstructural properties of 2024 and 7075 aluminum alloys which were joined together by friction stir welding. The rotating speed of the tool was 700 RPM while the welding speed was 2.67 mm/s. The 7075 alloy was on the advancing side of the tool while the 2024 alloy was on the retreating side. The authors concluded that 2024 and 7075 aluminum alloys were successfully joined by FSW and no superficial porosity or defects were observed in both weld top and rear surface. The tensile response, transverse to the welding direction, of the 2024 and 7075 AA joined by FSW was studied and the authors conclude that the tensile strength of AA 7075 T6 is the highest (600 MPa), the joint with the dissimilar alloys (AA 2024 T3 and AA 7075 T6) and joint of AA 2024 T3 has almost the same ultimate tensile strength but the toughness of AA 2024 T3 is very high and the elongation of the AA 2024 T3 specimen is very high compared to the weld of dissimilar alloys.

Research on the weld defects was done by Hua-Bin Chen, Keng Yan, Tao Lin [12] and they concluded that the defects such as lazy S, kissing bond and tunnel defect are due to the geometry of the tool, tilt angle, forged force and screw pitch of the tool. The reason for the tensile fracture in the butt welds is the initial oxide layer which gets stirred into oxide particles and distributed in the weld.

Hua-Bin Chen, Keng Yan [12], Tao Lin also researched and investigated on the ultimate tensile strength and elongation and concluded that these properties are very low when the tilt angle of the tool is 2^{o}, but no defects were found in the exterior of the weld. This observation lead them to study the fracture surface of the they found a single lap pattern with a interlayer spacing of 0.13 mm, they recognized this defect as the kissing bond. This kissing bond defect is the reason for the failure of many specimens in my research also. The reasoning given by the authors is that the nugget did not receive enough frictional heat to fuse the metal instead the layers of the metal as extruded by the metal has get stuck to each other and formed the kissing bond defect. The authors observed that this defect is extremely difficult to detect with non destructive methods.

Hua-Bin Chen, Keng Yan, Tao [12] Lin have also worked on a different kind of defect commonly found in FSW joints called the "lazy S". The defect is detected during the micro structure study which looks like broken and stirred black lines, which are due to the oxide layers on the initial butt joint surface. The study of the specimen under an EDS determined that this defect is due to Al2O3 particles.

T. Minton and D.J. Mynors [16] have demonstrated that a conventional vertical milling machine can be converted into a friction stir welding machine and sound welds can be fabricated, as they fabricated many welds with varying process parameters studied the micro structure and tensile tested the welds for the strength [16].

W. M. Thomas and E. D. Nicholas [15] have proposed the idea of a stationary weld head and moving anvil, the concept of caterpillar truck is utilized in order to move the material through the stationary head, the whole system works the same

way as the domestic sewing machine, the commercial use of this technique will reduce the time taken for joining process and increase the time efficiency, but the proposal does not talk how to provide the work pieces with sufficient clamping force and how to do the butt joints as they have considered only welding butt joints.

William D. Lockwood, Borislav Tomaz [9] have conducted the experiments on the sheets fabricated by friction stir welding and conducted the analysis using 2-D finite element model. The correspondence between the experimental results and the analysis was not cent percent, the authors conclude by explaining that the lack of correspondence between as the result of iso-stress loading assumptions in the analysis [9].

Therefore it is important to study the effects of friction stir welding process parameters on the mechanical properties of the joints and determine the optimum process conditions that would result in the desired microstructure and properties for sheet metal formed structures.

1.6 RESEARCH OBJECTIVES

The objective of this research is to characterize the mechanical properties of friction stir welded joints and study the micro structure of the base metal and the weld nugget evolved during the friction stir welding of similar and dissimilar alloys of Aluminum. Aluminum 2024 and 7075 are considered for this investigation. The mechanical properties such as ultimate tensile strength, yield strength, formability, ductility and vicor's hardness are measured and an effort is made to find out a relation between the process variables and properties of the weld. The optimal process parameters for the Friction-Stir welding of AA2024 and AA7075 will be defined based on the experimental results.

CHAPTER 2: EXPERIMENTAL PROCEDURE

2.1 FRICTION STIR WELDING MACHINE AND THE PROCESS

The machine used for friction stir welding was a conventional vertical milling machine generously donated by The Boeing Company which was transformed into a friction stir welding machine by designing a fixture that makes the milling machine capable of performing friction stir welding, the friction stir welding machine is shown in Figure 2-1.

Figure 2-1 Cincinnati vertical milling machine transformed into a friction stir welded machine for research the picture shows the fixture designed for the machine to transform it into a FSW machine.

The task of designing the fixture for the machine was taken up as a senior capstone project and was completed successfully and friction stir welded joints were fabricated on the machine. The final design was machined in the student machine shop and the final fixture set up on the machine is as shown in the Figure 2-2.

Figure 2-2 Fixture designed for transformed to transform conventional milling machine into a friction stir welding

The tool used for welding was a cylindrical tool with a threaded probe which also has a cylindrical cross section, the threads designed on the probe is for efficient stirring of the metal and efficient filling of the material in the gap formed during welding process. The tool used for welding is recommended by the Boeing Company and was ordered specifically from a vendor who manufactures the tools for Boeing Company. The tool used for fabrication of the welds in the research is shown in Figure 2-3.

Figure 2-3 Tool used for friction stir welding

Friction stir welding is done by holding the plates to be welded securely in the fixture designed so that the plates stay in place and do not fly away due to the welding forces. The rotational motion of the spindle is started and the tool is than got in contact with the surface of the plates and the probe is penetrated to a predetermined depth in between the faying surfaces of the plates to be welded.

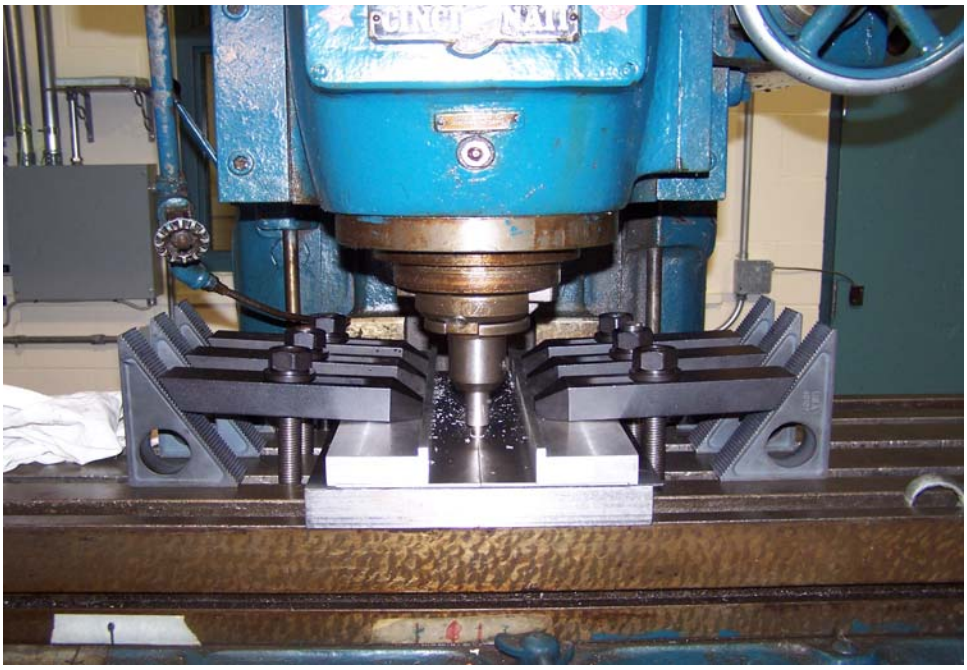

Figure 2-4 FSW machine fabricating the welds

The tool is given some time as it rotates in contact with the surfaces to soften the material due to the frictional heat produced, this time is called as dwell time, and after the dwell time the tool is given forward motion which formed the weld. The tool is with drawn after the weld is fabricated, the process leaves a hole and the design of the weld is done in such a way that the part with the hole in it is cut and not used for further processes with the welded plates. Efforts are on the way to retrieve the tool slowly from the weld to avoid the hole at the end. A figure of the FSW machine when the weld is being fabricated is shown in Figure 2-4.

2.2 TENSILE TEST SPECIME PREPARATION AND PROCEDURE

2.2.1 SAMPLE PREPARATION

The tensile tests are done on the fabricated welds according to the standards given by the Boeing Company, the beginning and the end of the welds with holes are sheared and not used for the research purposes. The welded plates are marked for the right dimensions and sheared in a manual shear to a width of ¾th inch. Generally two tensile specimens are cut from each welded joints to ensure accuracy. The specimens are marked for identification, the center of the weld is identified and half inch mark is made to facilitate the measurement of elongation after the test sample breaks under tension the specimens with the marking is shown in the Figure 2-5.

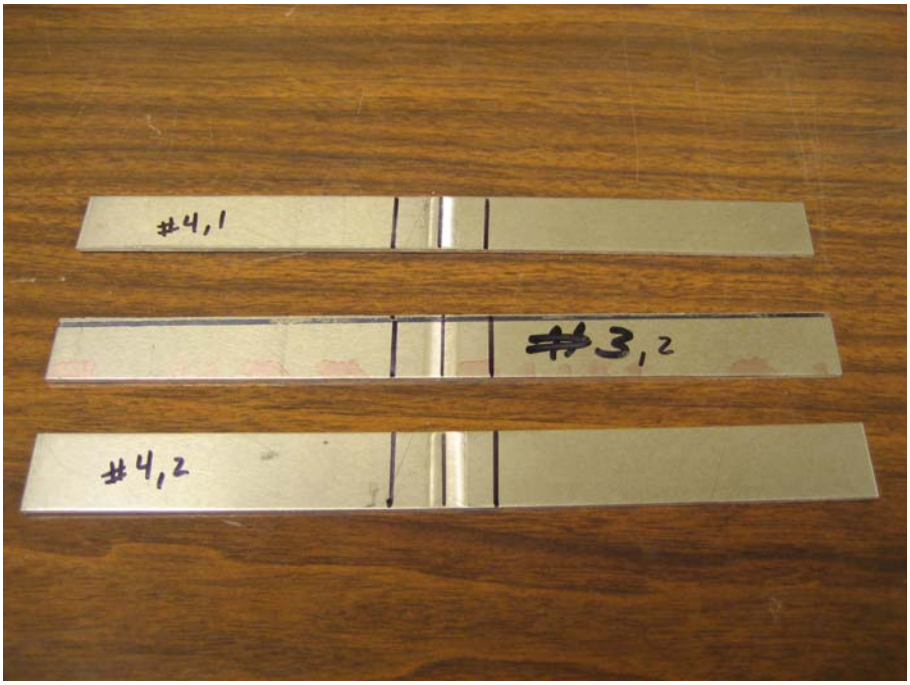

Figure 2-5 Tensile specimens marked and set ready for the testing

2.2.2 TENSILE TEST (MTS) MACHINE DESCRIPTION

The MTS machine used for tensile testing is a MTS system corporation manufactured machine with a capacity of 10 metric tons the machine is a hydraulic powered and water cooled. The MTS machine is very versatile and many different tests are run on this machine by changing the die set on the hydraulic actuator. Hydraulic wedge grippers are used for the tensile tests, the grippers are shown in the Figure 2-6.

Figure 2-6 Hydraulic wedge grippers used for tensile test on the MTS machine

The grippers have control for adjusting the griping force on the specimen and the grippers are equipped with rough surface to hold the specimens with out slipping. The MTS machine has a data acquisition system attached to it which helps record and save the data obtained during the testing process. The data from the acquisition system which is shown in Figure 2-7 can be retrieved and processed to obtain final results and graphs to estimate the behavior of the metal under different stresses.

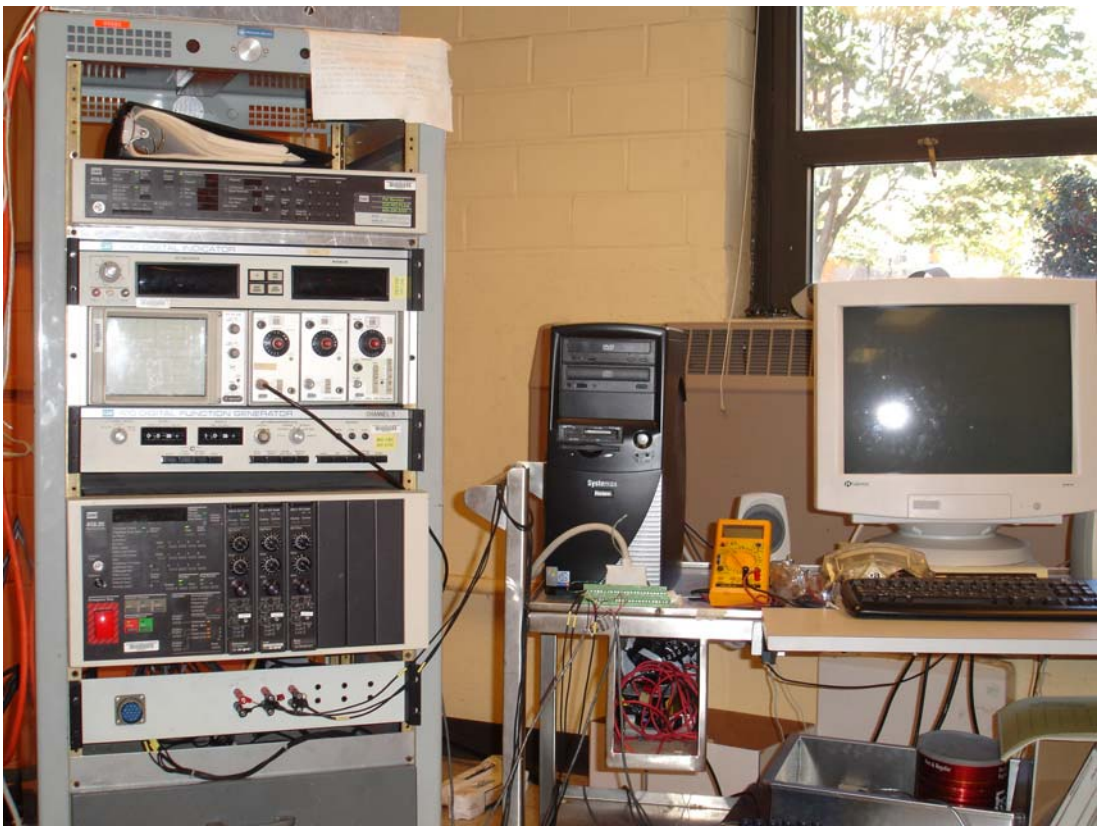

Figure 2-7 Data acquisition system for the MTS machine

The MTS machine has a controller panel attached to it which has all the knobs for the operation of the machine, the controller has a key pad which is used for programming and controlling the hydraulic actuator. The control panel also has a screen to display simulation of graph of the motion of the actuator even without

switching on the hydraulic system of the MTS machine. The machine has a capacity to work with different cartridges to meet the needs of the materials being tested. The cartridges can be changed with little effort and some changes in the controller values.

The MTS machine has the capability to accommodate an extensometer to indicate the elongation of the specimen in response to the tensile load applied. The extensometer used for research is also manufacture by MTS System Corporation. The extensometer is attached to the tensile specimen with the help of springs as shown in the Figure 2-8, so that the elongation of the specimen is proportional to the displacement indicated by the extensometer. The instrument has two holes which need to be concentric before the beginning of the experiments ensuring neutral position of the extensometer. The extensometer is disconnected before the specimen fractures to retain the accuracy of the instrument because the extensometer is very sensitive and may break due the shock during fracture of the specimen.

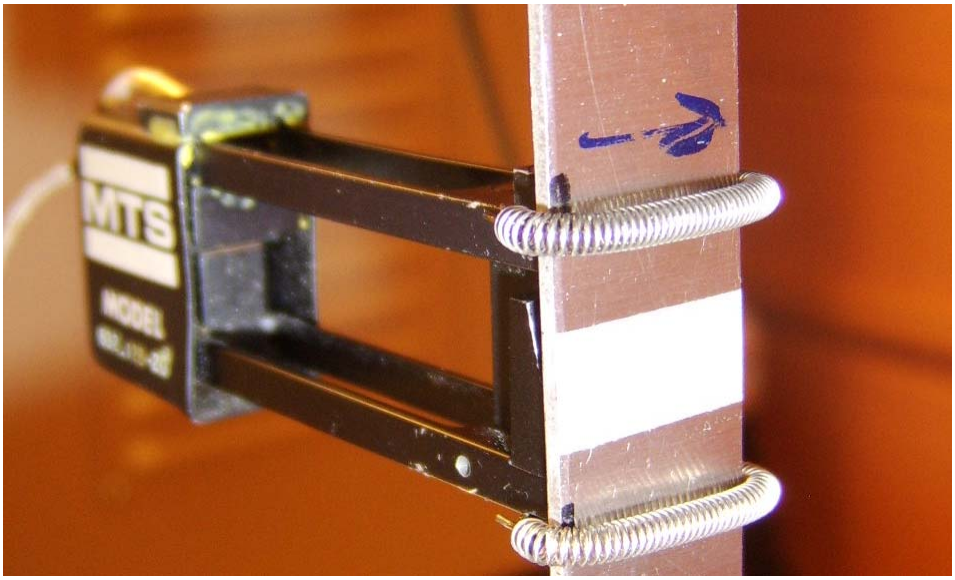

Figure 2-8 Extensometer attached to the tensile specimen using springs during testing

2.2.3 EXPERIMENTAL PROCEDURE

The experimental procedure is explained in a step by step manner in this section.

1. The cooling water is turned on to carry away the excessive heat from the oil as the machine is powered hydraulically.
2. The power cord is plugged into the socket on the wall.
3. The DC error is set to zero.
4. The hydraulic pressure is turned on, first the low hydraulic knob is turned on and then the high knob is turned on.
5. The program number is punched in the controller key pad to control the hydraulic actuator.
6. The controller is set to the Run Enable mode before starting the experiment.
7. The controller is checked to see if the "Output at 0" light is on. If not, the "Return to 0" button is turned on.
8. The load cartridge capacity is checked to see if it matches with the transducer full scale reading, if not the transducer full scale reading is changed to match the load cartridge number.
9. The extensometer is connected to the testing machine by inserting it in the right slot and then it is attached securely to the tensile specimen using springs or rubber bands.
10. The specimen with the extensometer is placed in between the grippers, after the grippers are set to correcting gripping pressure (if the gripping pressure is low the specimen will slip out of the gripper instead of applying tensile load on it, if the gripping pressure is too high the grippers will crush the specimens and breaks it before the experiment begins).

11. The experiment is started by turning on the run knob and the data acquisition system is also turned simultaneously so that the response of the material can be collected from the beginning of the experiment.

2.3 STRETCH FORMING PROCEDURE

The stretch forming experiment is also conducted on the same machine as the tensile test, the hydraulic grippers are replaced by the stretch forming die to transform the machine to perform the stretch forming. The die is as shown in Figure 2-9.

Figure 2-9 Close up view of stretch forming die figure shows the die set (base), top plates and the punch

The figure shows the die which constitutes the die set, top plates and the punch. The specimens for the stretch forming are cut on a shear to a width of 2 in. The specimens are placed in the center of the slot of the die set by drawing lines on the die set and on the specimen in the center and making the lines to coincide with each other. The top plates are placed with out disturbing the plate position on the die set

and the four screws are tightened simultaneously to ensure equal force on all the sides of the plate. The machine is switched on and the errors are got down to zero and the die set is made to move to touch the punch. Punch is the stationary part which is attached to the load cell to read the force on the plate, the die set is fixed to the hydraulic actuator and its motion can be controlled by the knob on the controller. The die set is moved towards the punch and a paper is used to find out if they are in contact, if the paper can be drawn with a drag on it because of the punch and the specimen in contact it indicates the set up for the experiment is ready and the experiment can be run by hitting the run button on the control panel of the machine. Figure 2-10 shows the experimental set up before the beginning of the experiments.

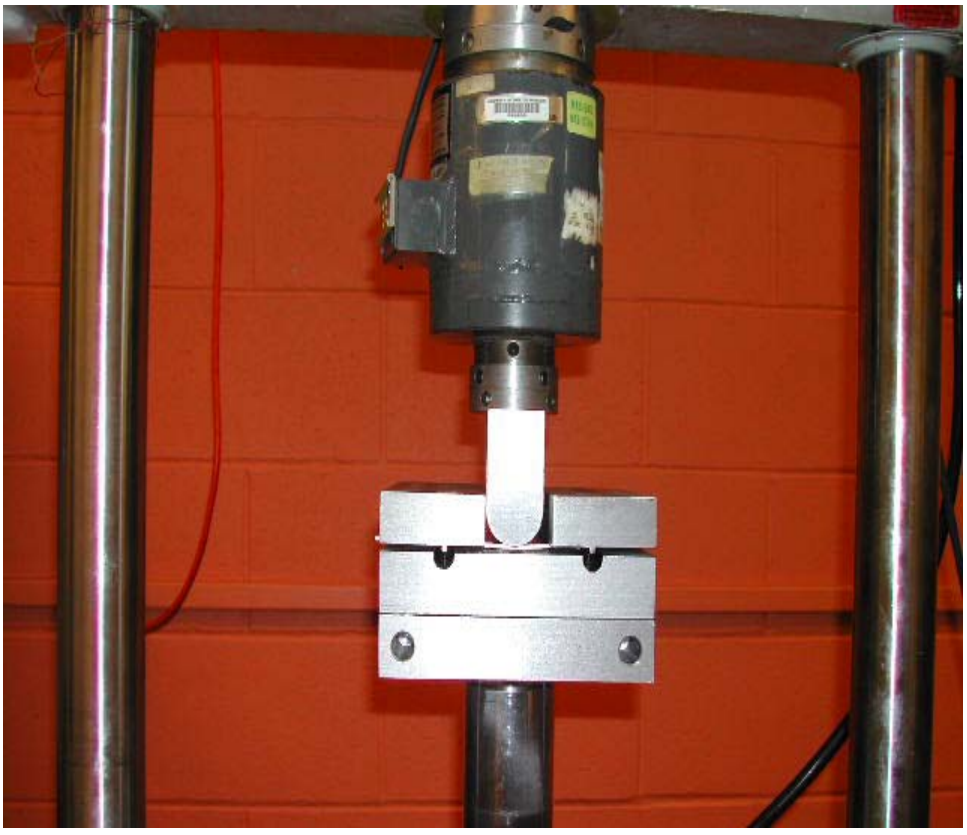

Figure 2-10 Experimental setup for the stretch forming process

The experiment is started and run until the specimen breaks or there is cracking sound. The data acquisition system is switched on and off simultaneously with the MTS machine in order to collect data precisely on the load is exerted on the specimen. The samples which were ductile have formed and taken the shape of the die, but the specimens from materials like AA 7075 – T6 have just bent but did not form examples for the ductile and the brittle samples are shown the figures below.

Figure 2-11 Specimen after the stretch forming of AA 2024-T3, the sample has formed to take the shape of the punch of the stretch forming die

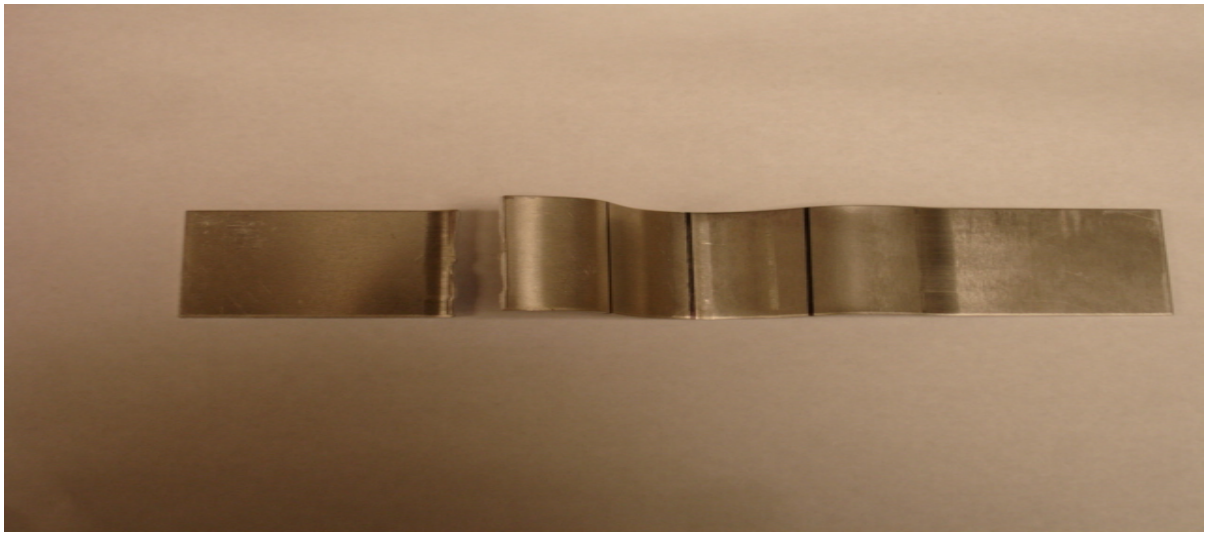

Figure 2-12 Fractured specimen of the stretch forming from AA 2024 T-3

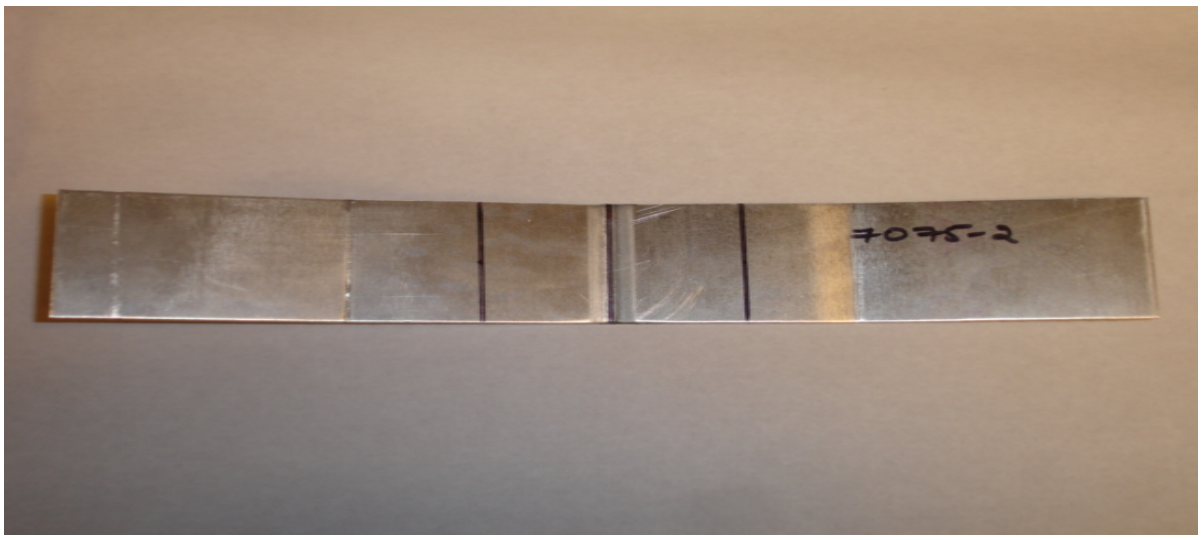

Figure 2-13 Stretch formed sample of AA 7075 T-6, the sample has not taken the shape of the punch.

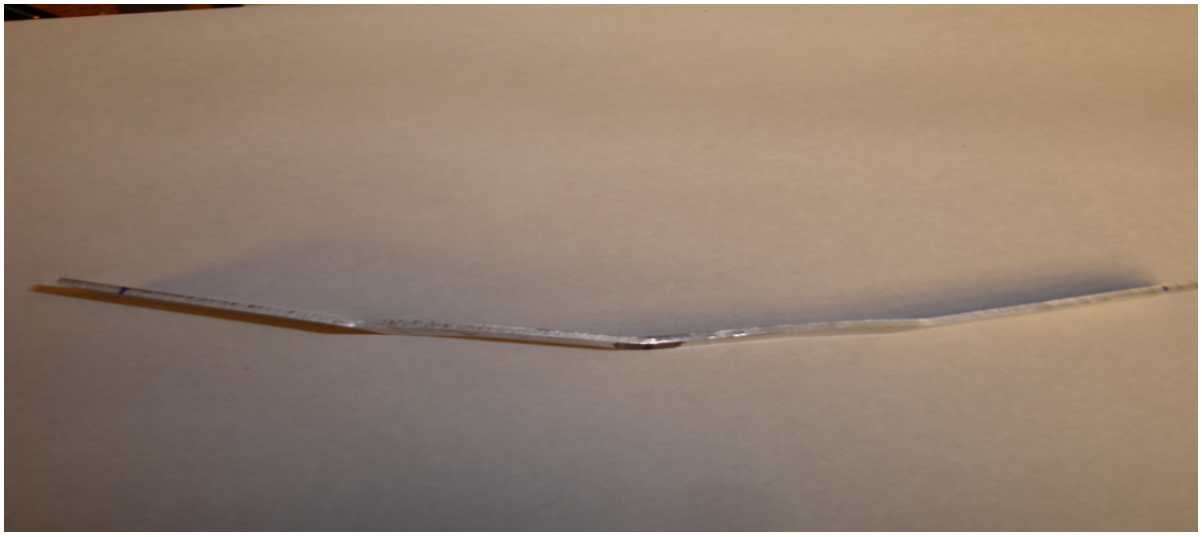

Figure 2-14 Side view of the brittle sample of (AA 7075 T-6) which has bent and cracked under the stress due to stretch forming

The data is collected from the acquisition system and processed for the force, displacement and time taken for the deformation. The thickness of the samples is measured for the thinning in the weld section due to the stretch forming.

2.4 VICKERS MICROHARDNESS TESTING

The microhardness of the welded joints was measured on a Buehler micromet II micro hardness tester. The micro hardness tester has an eyepiece and a rhombus shaped indenter to measure the micro hardness of the material. The load on the

Figure 2-15 Buehler micromet II micro hardness tester

indenter can be set using a knob on the tester. The Figure 2-15 shows the micrometer which works in conjunction with the eyepiece to measure the indentation

dimensions. The time of indentation can be set by using the knob on the front panel of the micro hardness tester as shown in Figure 2-15.

The sample whose micro hardness is to be measured in mount in phenolic powder and fixed securely on the table shown in the figure, the eyepiece is used to locate the point where the measurement is to be taken and the height of the table is adjusted until the a clear image of the specimen is seen in the eyepiece then the table is locked in this height and the eyepiece is removed and the indenter is put in place above the sample. The time of indentation and the load on the specimen are set to desired numbers and the start button on the front panel of the instrument is turned on. The indenter indents the material and leaves a rhombus shaped dent on the surface of the sample. The indenter is then pushed back so that the eyepiece is right on the sample. The dimensions of the diagonals are measured and the average of the measurements is calculated and substituted in the formula to calculate the hardness number. The formula used is $H_v = 1.854\ F/d^2$ where F is load in kgf, d is the average of the two diagonals of the indentation.

2.5 SAMPLE PREPARATION FOR STUDY OF MICROSTRUCTURE UNDER OPTICAL MICROSCOPE

The samples mounted for micro structure study are cut from the weld in transverse and longitudinal directions to study the weld structure in detail in both directions. A piece of 5mm X 2mm X 2mm is cut from the welded sheets along and across the weld. The samples are ground on a grinder to smoothen the edges and get an even surface for surface for studying the micro structure. Mounting is done on a Buehler automatic mounting press with black phenolic powder. The mounting press is shown in the Figure 2-16.

Figure 2-16 Buehler automatic mounting press used for mounting the samples for the microstructure study.

The press is pneumatic and works on compressed air, the compressed air valve is turned on and the on switch is pressed. The mounting press has many options on the front panel (as can be seen in the Figure 2-15) to suit the material, size and temperatures of the materials being mounted. The material knob is set to thermo setting, mold size is set to 30mm, heating time is set to 5 min, cooling time is 3 min, pressure is set to p.s.i., temperature is set 270^{o}C and the pre load is set to p.s.i. The samples are set on the top of the ram and then two scoops of powder is put on top of the specimens and care is taken not to put too much powder and tilt the sample, as the surface for inspection will be at an angle and desired images and results can not be got. The ram is taken down by pressing the down arrow and the handle is compressed and closed to seal in the pressure. The cycle start button is pressed and the mould is taken out after 8 min including 3 min for water cooling. The resulting moulds are as shown in the Figure 2-17.

Figure 2-17 Samples mounted in phenolic powder on the automatic mounting press with some powder on the samples which can be removed by polishing

The mounted samples are polished on polishing paper of grit 400, 600 and 800 with a combination of water and diamond paste for smooth finish, the final stage of polishing is on smooth cloth with a diamond suspension liquid for smooth finish.

The samples are etched after polishing to reveal the microstructure clearly; the acids in the etchant attack the grain boundaries and give a clear image of the size of the grains. The etchant used for aluminum alloys is Keller's etchant which is prepared by adding 1 percent of hydrofluoric acid by volume, 1.5 percent of hydrochloric acid by volume, 2.5 percent of nitric acid by volume and 95 percent of distilled water by volume. The samples are etched for 1 min according to the Boeing company standards, but overetched for one more minute if the microstructure is not revealed.

The etched samples are washed thoroughly to remove the carbon deposits and pat dry to study the microstructure under the optical microscope.

2.6 STUDY OF MICROSTRUCTURE UNDER OPTICAL MICROSCOPE

The optical microscope used for the study of the microstructures is a Nikon model Epiphot 200 and is shown in the Figure 2-18. The optical microscope works in conjunction with a computer built by Buehler which has Enterprise (image analysis software) installed in it.

Figure 2-18 Optical microscope and the data acquisition computer used for the study of the microstructures

The microscope has 5 X, 10 X, 20 X, 50 X and 100 X magnifications to facilitate the detailed study of micro structures of the samples. The microscope is equipped with a knob to control the intensity and brightness of the bulb on the Nikon power unit

which is also attached to the micro scope. The microscope is attached to a display unit which gives a bigger and clear view of the microstructure but the display unit does not have the capability to record the images. The computer which is the data acquisition system for the microscope has the software required to capture and store the images taken on the micro scope. The images are copied on to a Microsoft word document and then transferred to other computer through a zip disk for processing and study of the image.

2.7 STUDY OF MICROSTRUCTURES UNDER SCANNING ELECTRON MICROSCOPE AND ENERGY DISPERSIVE SPECTROSCOPY

The study of the microstructures under the Scanning Electron Microscope (SEM) needs careful sample preparation, without which the electrons from the electron gun of the microscope will stick to the sample. The electrons stuck to the sample form a shiny coat on the sample hiding the microstructure under them. The samples should be mounted and fixed to a stainless steel stand as the SEM needs a conductive loop from the samples to study the micro structure of the sample. Silver paint is painted to the end of the sample and connected to the stainless steel stand in the bottom of the sample to form the conductive loop. Then the sample is put inside the vacuum chamber and the air is pumped out until the chamber reaches the desired vacuum.

The magnification is set to clearly identify the different zones, grain boundaries and defects. The microscope has the capability to perform EDS which used the same image from the microscope and analyses the chemical composition of the targeted spot or area.

CHAPTER 3: RESULTS AND DISCUSSIONS

A wide range of welds were run for spindle speeds ranging from 800 rpm to 1300 rpm, feed rate of the spindle ranges from 2.125 in/min to 7.625 in/min, and the plunge depth ranges from 0.075 in to 0.104 in. The head pin used was threaded and made of non consumable high carbon steel. The dwell time was maintained constant for all the cases as 15 sec. The research focus was to weld similar and dissimilar welds of AA2024-T3 and AA7075-T6. Three different cases were studied which is welding of AA2024-T3 for both plates, AA 7075-T6 for both plates and welds of dissimilar welds of AA2024-T3 and AA7075-T6 on each side. The three cases are studies separately and tested for strength, formability, ductility and micro hardness. The microstructures of all the cases are studied under optical microscope, scanning electron microscope and energy dispersive spectroscopy (EDS).

3.1 Welding of Similar Materials

3.1.1 Case 1: 2024

In order to design a set of experiments to capture the impact of the process parameters (rotational speed, feed rate and plunge depth), response surface methodology (RSM) was used. Response surface methodology was invented by G. E. P. Box and K. B. Wilson in 1951 [13]. Response surface methodology is used to explore the relationships between several response variables. This technique is used to obtain the optimal response from the response variables. The technique is easy to

apply and the resultant model of experiments is easy to estimate. The following set of experiments listed in Table 3-1 was designed using the RSM method.

Sample number	Rotational Velocity of Tool (rpm)	Travel Velocity of Tool (in/min)	Plunge Depth (in)
1	1300	2.125	0.075
2	1300	3.625	0.078
3	1300	5.75	0.080
4	1300	7.625	0.078
5	**1045**	**5.75**	**0.080**
6	1045	3.625	0.075
7	1045	7.625	0.080
8	840	4.625	0.075
9	840	5.75	0.078

Table 3-1 L9 array showing the different combinations of the process parameters

The L9 array for AA 2024-T3 was formed by selecting three different values for the three process parameters which are rotational speed, feed rate and plunge depth. The values selected for spindle speed are 840 rpm, 1045 rpm and 1300 rpm. 840 rpm and 1300 rpm were selected as they are the extremes of the range and 1045 is selected as this spindle speed resulted in the good weld in initial set of test welds fabricated. The feed rated selected for the L9 array are 2.125 in/min and

7.625 in/min as they are the extreme values of the range and 5.75 in/min as the weld fabricated at this feed rate have yielded good tensile strength and percent elongation in the preliminary set of experimental. The penetration depth used for the array is 0.075 in, 0.078 in and 0.080 in. The penetration depth above 0.080 in has not resulted in welding between the plates.

Sample Number	Ultimate Tensile Strength (MPa)	Ultimate Tensile Strength (psi)
1	324.28	47032.92
2	437.66	63477.33
3	407.01	59031.92
4	429.48	62290.92
5	**449.86**	**65246.79**
6	445.23	64575.27
7	424.62	61586.04
8	418.08	60637.49
9	424.73	61601.99

Table 3-2 Table showing ultimate tensile strength from the tensile test in psi and MPa

Table 3-2 shows the results of the tensile test and indicates the ultimate tensile strength in psi and MPa. It can be observed from the Table 3-1 and Table 3-2

that the combination of spindle speed of 1045 rpm, weld velocity of 5.75 in/min and plunge depth of 0.080 (i.e. experiment 5 in the L9 array of design of experiments) yields the highest ultimate tensile strength of 449.86 MPa and a percent elongation of 18.18. Thus, it is concluded that the combination of this process parameters with the dwell time 15 sec will result in a weld with good mechanical properties and micro structural characteristics.

Sample Number	Percent elongation	Yield Strength (MPa)
1	12.37	211.52
2	16	319.36
3	10.67	313.17
4	6.49	301.38
5	**18.18**	**309.75**
6	11.4	330.66
7	8.49	314.57
8	12.73	303.69
9	11.18	310.56

Table 3-3 Table showing percent elongation and yield strength in MPa

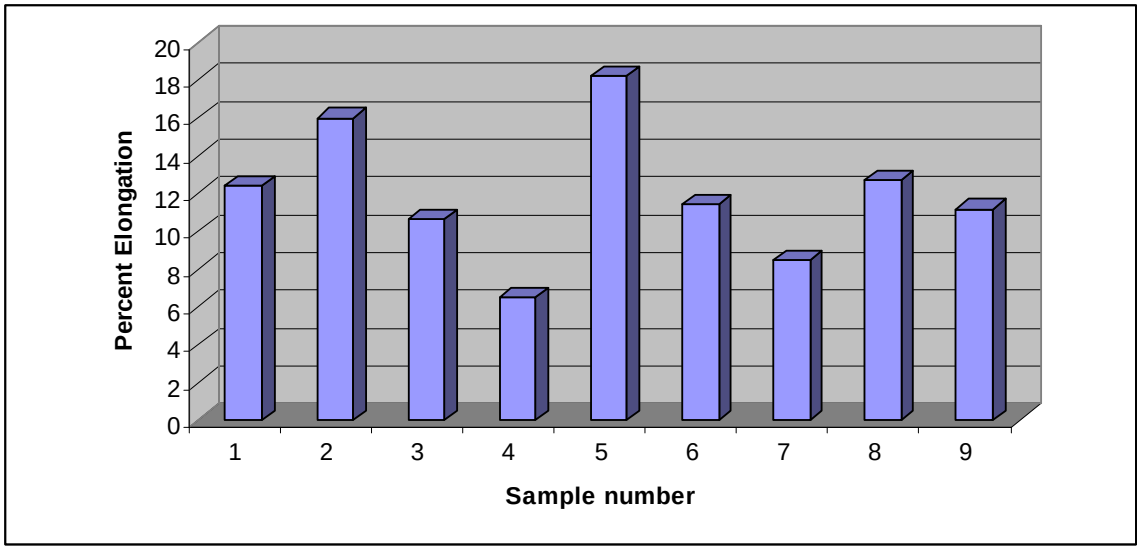

Figure 3-1 Column graph displaying the percent elongation of the samples fabricated from the L9 array of AA 2024-T3

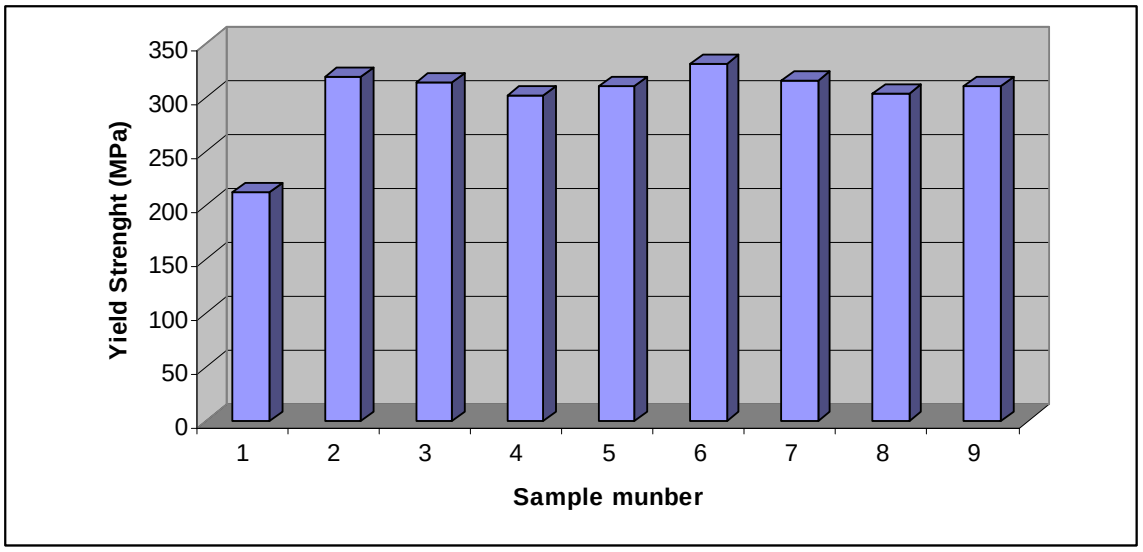

Figure 3-2 Column graph displaying the yield strength (MPa) of the samples fabricated from the L9 array of AA 2024-T3

The Figure 3-1 and Figure 3-2 compare the percent elongation and the yield strength (MPa) of all the nine samples with each other which are fabricated using the L9 array for AA 2024-T3.

The spindle speed of 1045 rpm, weld velocity of 5.75 in/min and plunge depth of 0.080 in gives the best combination of strength and ductility (high toughness). All the results were fitted to three dimensional surfaces in Statistica relating the effect of the independent variables (rotational speed and feed) to ductility of the joint. A typical presentation of response surface for ductility is displayed in Figure 3-3. In this plot, ductility of the joint as measured by the percent reduction of area was selected as the major response.

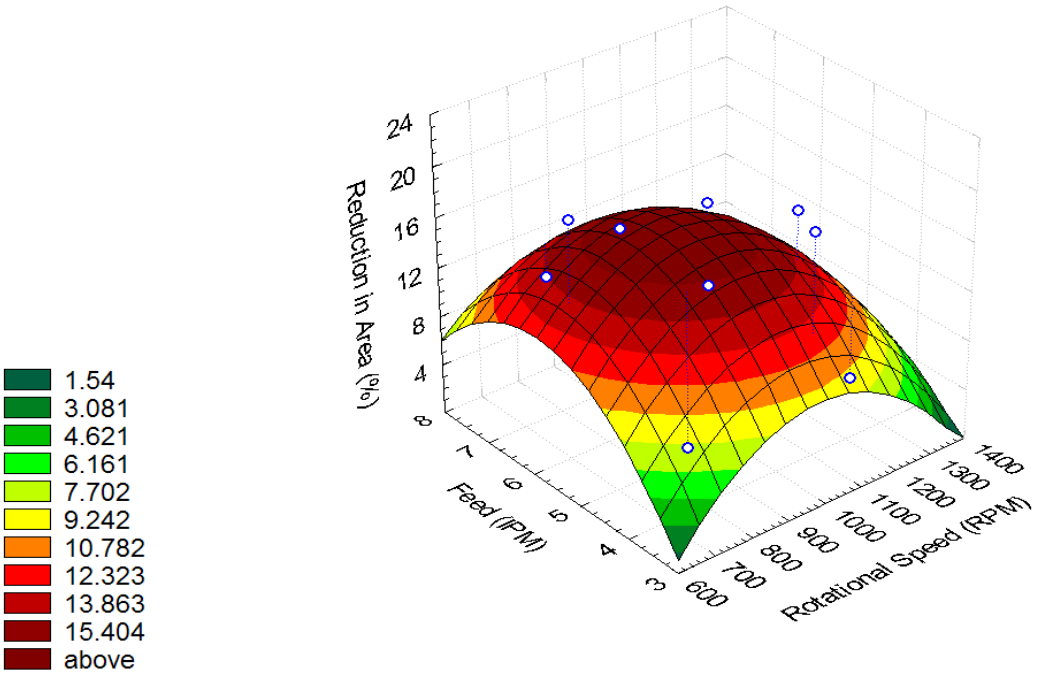

Figure 3-3 Surface plot of the effect of process parameters on ductility of FSW joints

The process contour map for joint ductility extracted from the surface plot is shown in Figure 3-4. Both Figures indicate that rotational speed in the range of 800 to 1100 rpm and welding speed of 4.5 - 6.5 inch/min would yield optimum joint ductility.

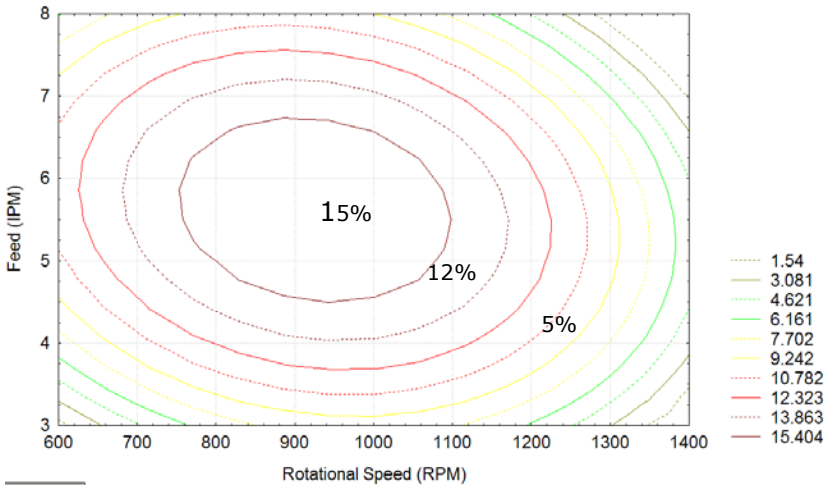

Figure 3-4 Process contour map for ductility of FSW joints

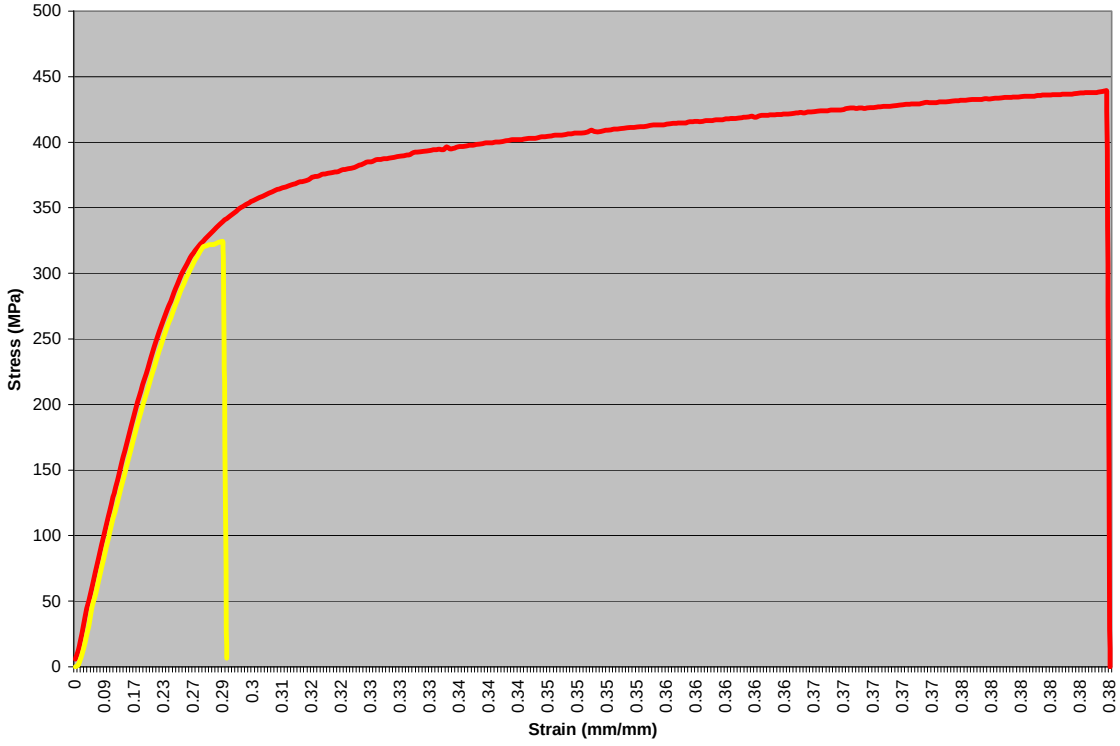

Figure 3-5 Graph showing the Stress-Strain curves of the best weld and the bad weld

The stress-strain curve is shown for the best weld and the bad weld superimposed on each other in the Figure 3-5. The area under the stress strain curve represents toughness which is the energy the material can take before rupture.

Formability of a joint is the relative ease with which a metal can be shaped through plastic deformation, this property is very important for the automotive and aerospace industry as the sheets of metal are welded first and formed to shape to form the particular shape of the die used for forming. Formability test results are shown in the Figure 3-6. It can be seen from the Figure 3-6 that the depth of the formed sample is maximum for the combination of spindle speed of 1045 rpm, weld velocity of 5.75 in/min and plunge depth of 0.080 (experiment #5). Some stretch formed samples are shown in the Figure 3-6.

Sample Number	Depth of formed sample (in)
1	0.80
2	0.42
3	0.63
4	0.45
5	**1.20**
6	0.3
7	0.46
8	0.25
9	0.95

Table 3-4 Table showing the formed depths of the joint after stretch forming

Figure 3-6 Front and side views of the stretched formed samples

The micro hardness of all the samples was the same except that there were changes from the base metal to HAZ and weld area. The microhardness was low in the HAZ area in the range of 95 H_v to 105 H_v, the range of microhardness in the nugget zone was from 115 H_v to 125 H_v and the base metal's micro hardness ranged from 130 H_v to 135 H_v.

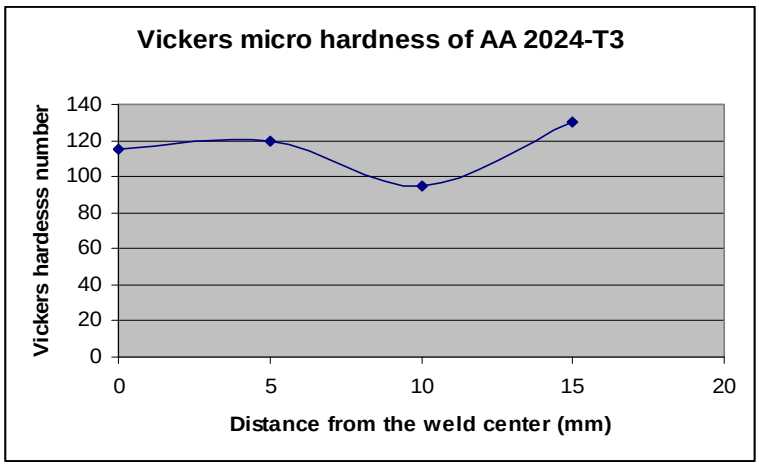

Figure 3-7 Graph showing the changes in the micro hardness of AA 2024 form the weld center to the base metal

The Figure 3-8 shows the base metal, HAZ and the fine crystalline weld nugget. The fine grains in the nugget zone are due to dynamic recrystallization of the metal during the welding process which is due to the frictional heat produced during the process between the shoulder and the work piece surfaces.

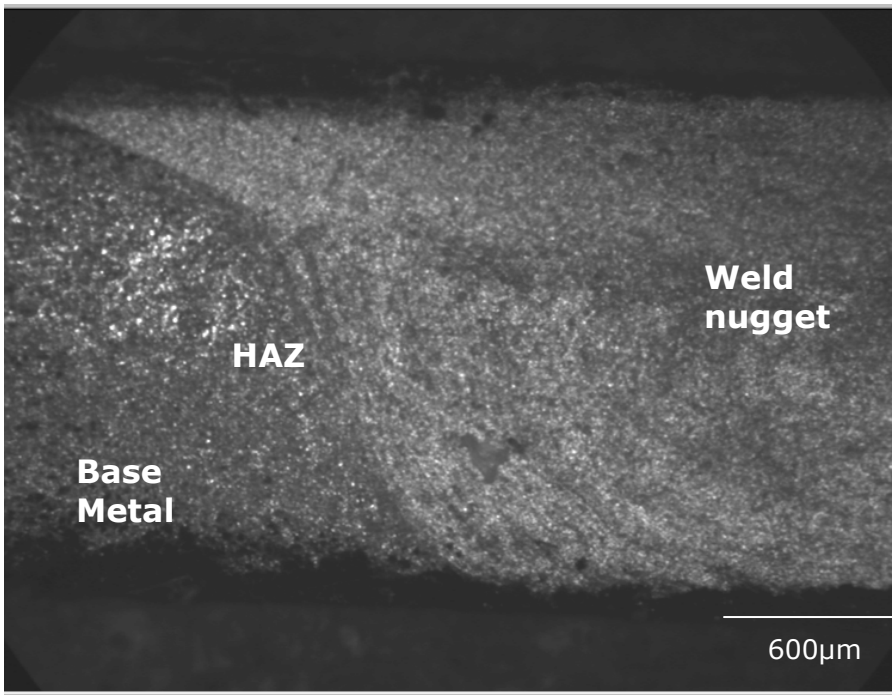

Figure 3-8 Image at 5X magnification of AA 2024–T3 showing the base metal, HAZ and weld zone

It can be seen that the base metal has larger grains and there is no much difference between the grain size of grains in the base metal and the HAZ, and there is clear distinction between the heat affected zone and the weld nugget. The micro structures of the welded joints and base metal were studied under optical microscope and scanning electron microscope. The optical microscope image of the weld zone of AA 2024-T3 in the experiment 5 of design of experiments is shown in the Figure 3-8.

Figure 3-9 shows clear distinction between four zones of the welded joint, thermo mechanically affected zone is also visible in this image. It can be noted that there is partial recrystallization in the thermo mechanically affected zone (TMAZ). The grains in TMAZ are affected by the motion of the tool and frictional heat generated by the tool, but did not receive enough heat to get recrystallized completely.

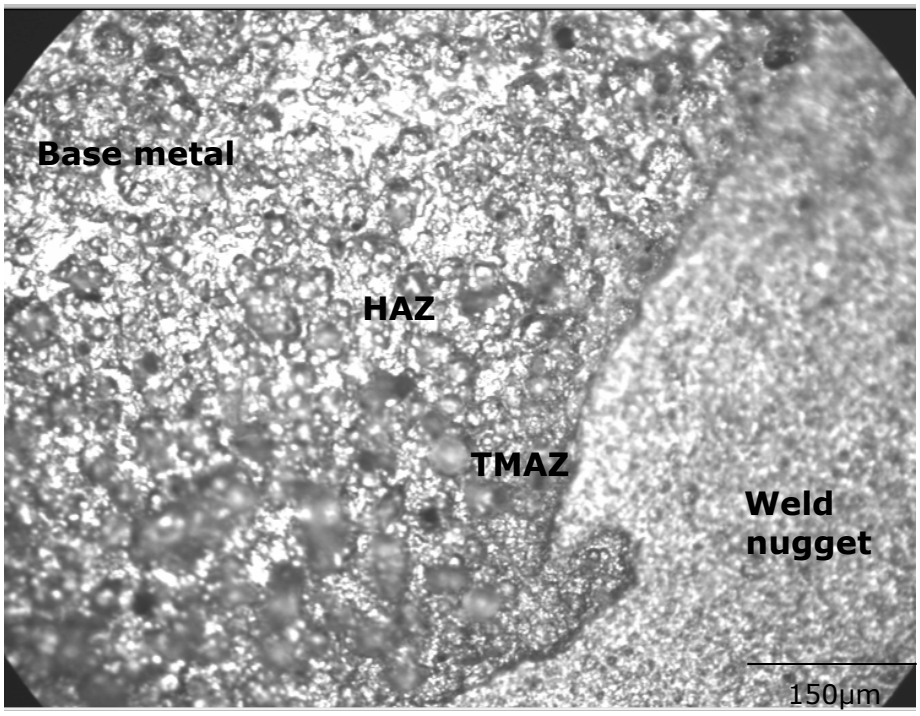

Figure 3-9 Image of AA 2024–T3 taken at 20X magnification showing the base metal and the weld nugget

There is no recrystallization in HAZ so the grains look same as the base metal but there is drastic change in the micro hardness of the heat affected zone compared to the base metal.

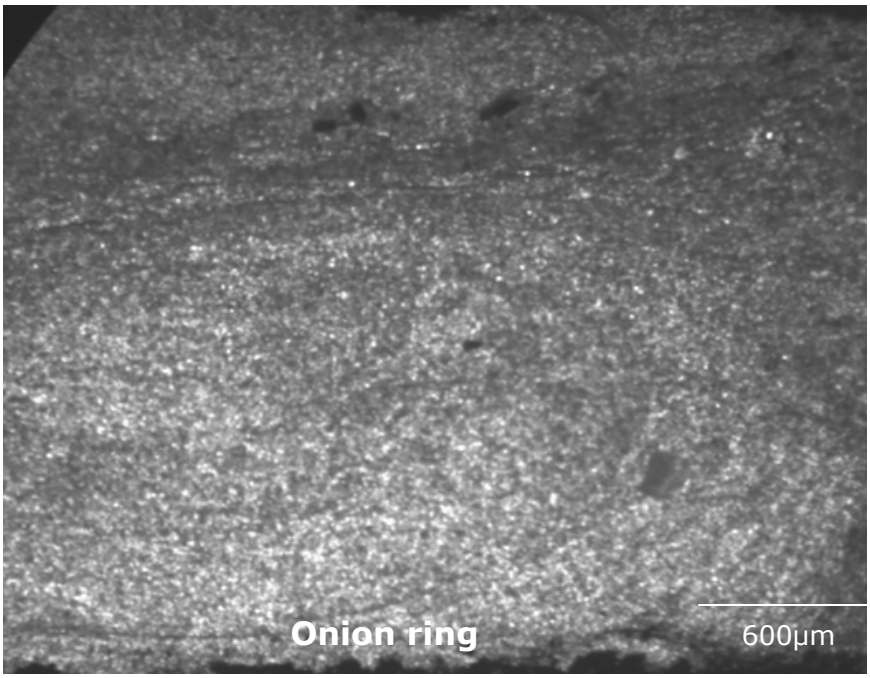

Figure 3-10 Image at 5X magnification of AA 2024–T3 showing the onion ring formation

Figure 3-10 shows the onion ring formation which is formed due to the extrusion of cylindrical sheets of metal with every rotation the tool moves forward. These rings are the characteristic features of the nugget zone and can be seen in the cross section of the nugget zone.

Figure 3-11 shows the voids formed due to the tool not being able to reverse forge the material into the gap created due to the forward motion of the tool in a bad weld of the design of experiments. The image shows the voids filled with phenolic powder while mounting the sample. Figure 3-12 shows the voids in a higher magnification of 10X it can be seen that the average width of the void is around 300µm. Figure 3-13 is a scanning electron microscope image showing the AA 2024 –

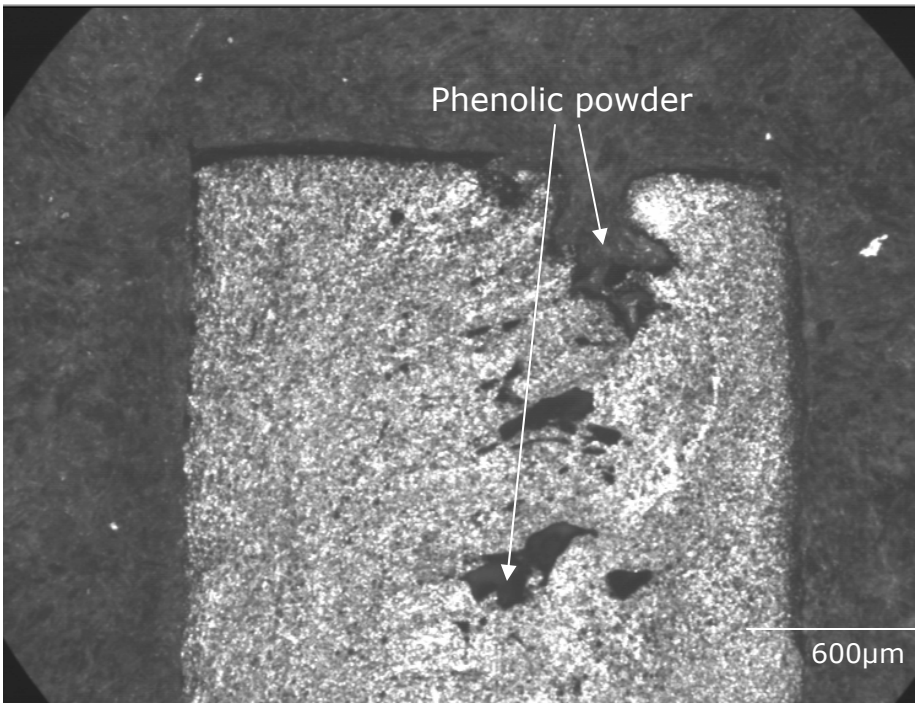

Figure 3-11 Image showing the defects formed in bad weld of design of experiments in AA2024- T3 at 5X magnification

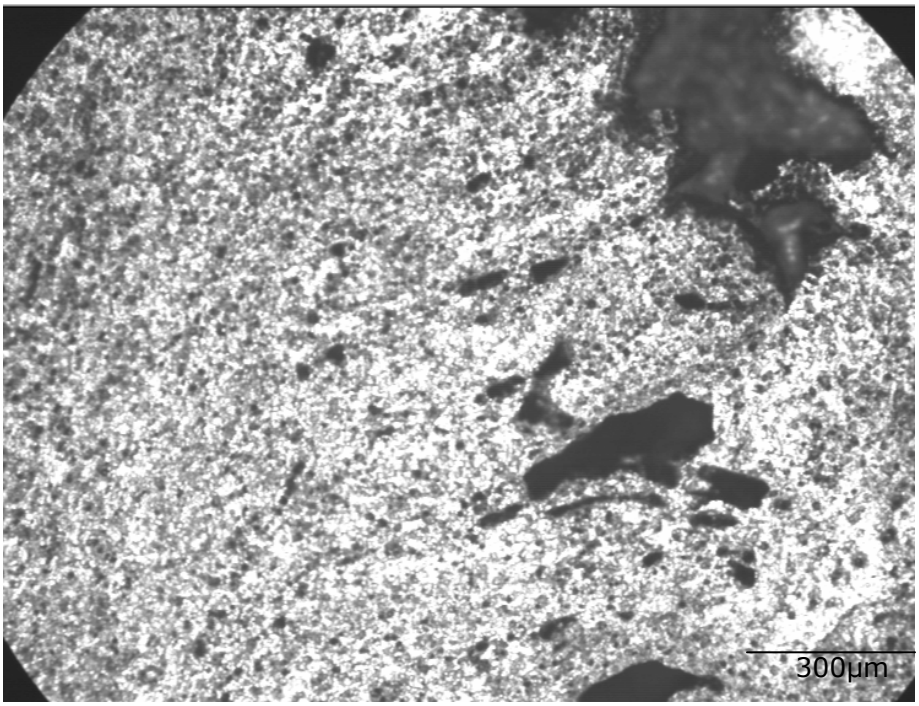

Figure 3-12 Image showing the defects formed in bad weld of design of experiments in AA2024- T3 at 5X magnification.

T3 specimen in the middle with many voids and the shiny coat around the sample is the layer of electrons which are emitted by the scanning electron microscope for its working. The electrons hitting the sample are not allowed to stick to the sample by forming a conducting loop around the sample using silver paint and steel stand.

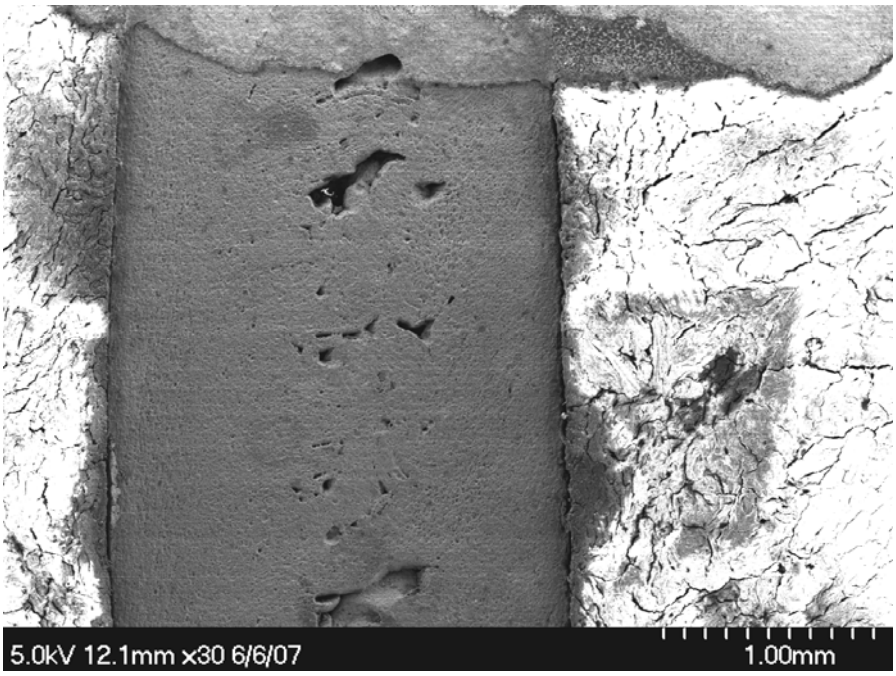

Figure 3-13 Scanning electron microscope image showing the defects formed in bad weld of design of experiments in AA 2024 – T3.

The study of failed tensile specimens provides in depth understanding of the process of failure in the specimens. Fractography of a sound weld of AA 2024-T3 in Figure 3-3-14 reveals the dimple elongated and voids which are microscopic on the fracture surface, which indicates a ductile failure due to the elongation of dimples and presence of voids of different sizes and shapes. It is also observed that the failure generally starts on the advancing side of the weld as there are more stresses on the advancing side than the retreating side as the transition from weld nugget to base metal is clear on the advancing side and not very distinctive on the retreating side. Figure 3-3-15 shows the elongated walls of the dimples due to the tensile force

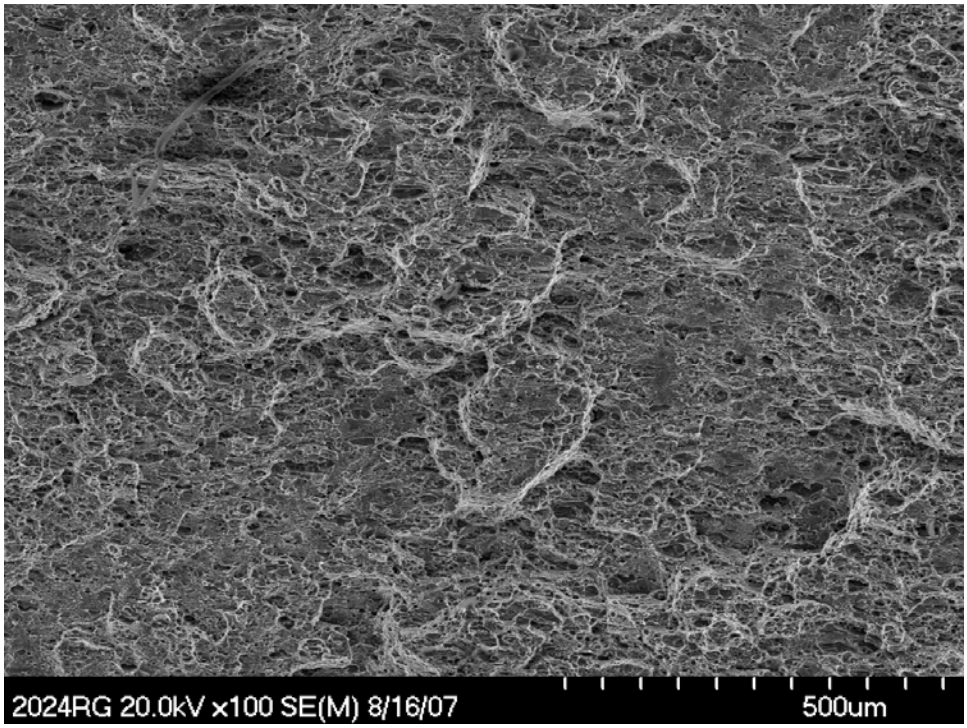

Figure 3-3-14 Scanning electron microscope image of fractured tensile sample of good weld showing overall morphology of the fractured surface.

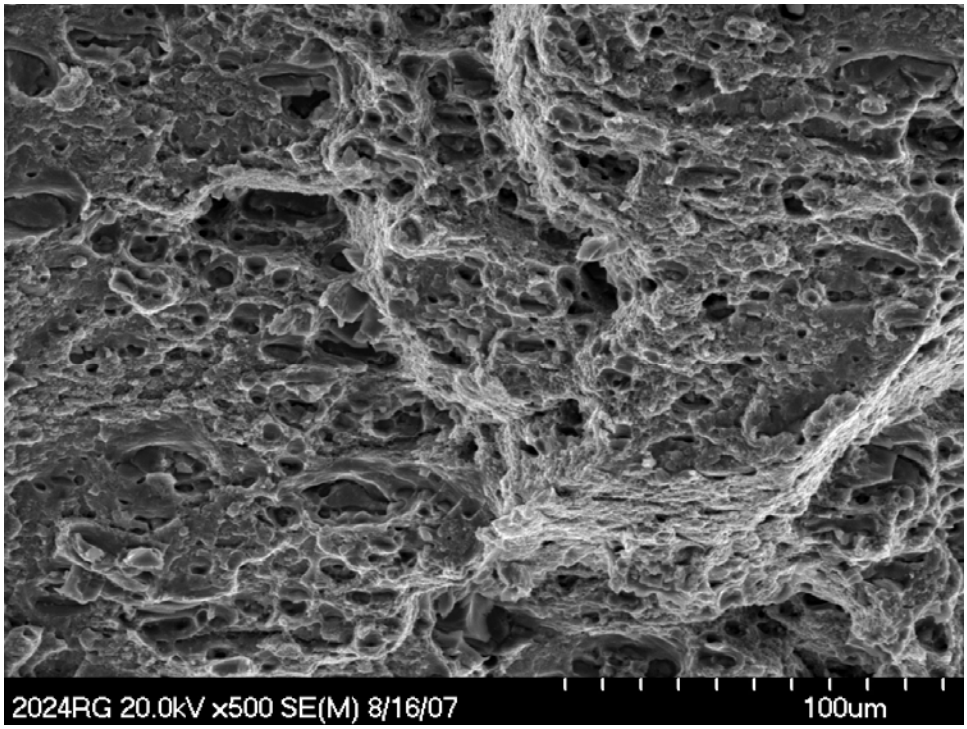

Figure 3-3-15 Scanning electron microscope image of fractured tensile sample of good weld at higher magnification

applied during the tensile test at higher magnification and it can be clearly seen that the specimen has failed due to ductile fracture from the microscopic level.

The fractography of a bad weld of AA 2024-T3 (experiment #6) reveals the kissing bond in the fracture location which indicates that there was no sufficient heat generation for the weld nugget to form, due to the deficiency of frictional heat generated during welding by the tool the metal around the tool could not infuse and recrystallize, instead the cylindrical layers of the metal extruded by the tool has stuck to each other and formed a kissing bond instead of a weld nugget.

Figure 3-3-16

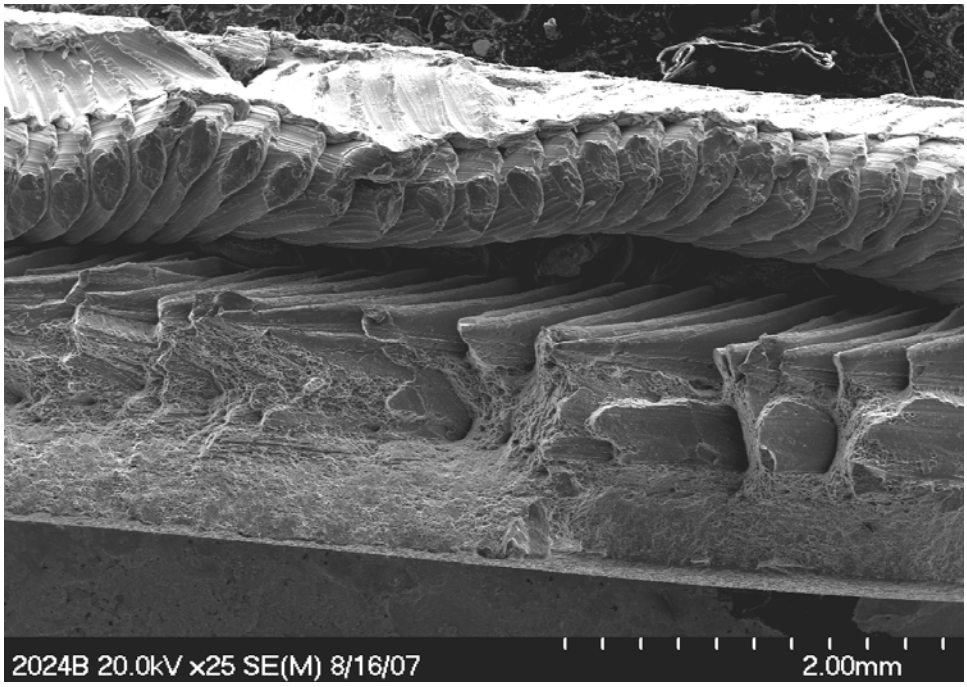

Figure 3-3-16 Scanning electron microscope image of fractured tensile sample of bad weld showing the kissing bond

and Figure 3-3-17 shows the fractured surface of a bad weld which show the kissing bond which is the reason for failure. The Figure 3-3-17 shows the kissing bond at

higher magnification which clearly shows the layers of extruded aluminum arranged on each other due to lack of frictional heat generated to form a weld nugget.

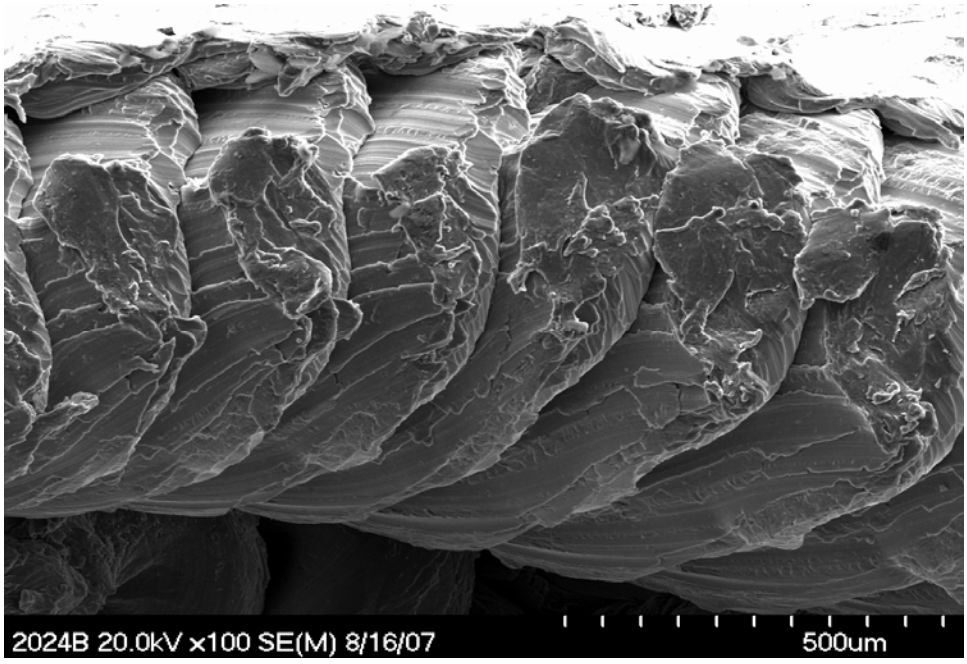

Figure 3-3-17 Scanning electron microscope image of fractured tensile sample of bad weld showing the kissing bond at higher magnification

3.1.2 Case 2: 7075

Three different combinations of process parameters were used to fabricate welds with AA 7075- T6. The process parameters are shown in the table below.

Sample number	Spindle speed (rpm)	Feed (in/min)	Plunge depth (in)
1	1045	5.75	0.080
2	840	7.625	0.080
3	1300	2.125	0.080

Table 3-5 Table of different combinations of process parameters used to weld AA 7075-T6

The first set of process parameters was tried as it resulted in the best weld characteristics for AA 2024-T3, the second and the third cases were tried as a combination of high speed – low feed and low speed – high feed. The results of the tensile test are as shown in Table 3-6. A combination of low speed - high feed (experiment #2) has worked flawlessly for AA 7075-T6 as can be seen in table below that the ultimate tensile strength is 440 MPa, there were no bad welds fabricated there were very few voids spotted in the microstructure study.

Sample number	Yield Strength (MPa)	Ultimate Tensile Strength (MPa)	Percent elongation
1	360	365	5.9
2	360	440	7.5
3	330	345	3.5

Table 3-6 Table indicating the yield strength, ultimate tensile strength and percent elongation for AA 7075-T6

The micro hardness of the welds is uniform and does not show significant changes for different weld zones, it varies from 155 H_v to 170 H_v.

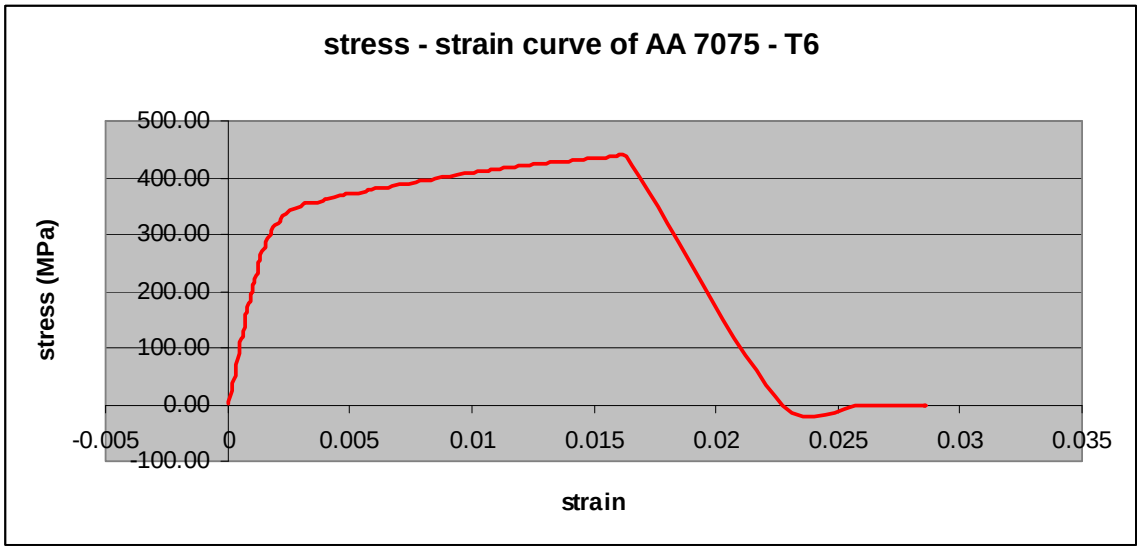

Figure 3-18 Stress – strain curve of AA 7075–T6

Figure 3-18 shows the stress–strain curve of the low speed-high feed combination which resulted in good weld. The stretch forming results of the AA 7075 – T6 is listed in the table below. Figure 3-19 show the morphology of the weld at 5X magnification which shows the base metal, HAZ and weld nugget. Figure 3-20 shows the SEM image of AA 7075-T6 in which the grains boundaries in the weld nugget can be identified.

Sample number	Depth of formed sample (in)
1	0.35
2	0.4
3	0.3

Table 3-7 Results of stretch forming of AA 7075–T6

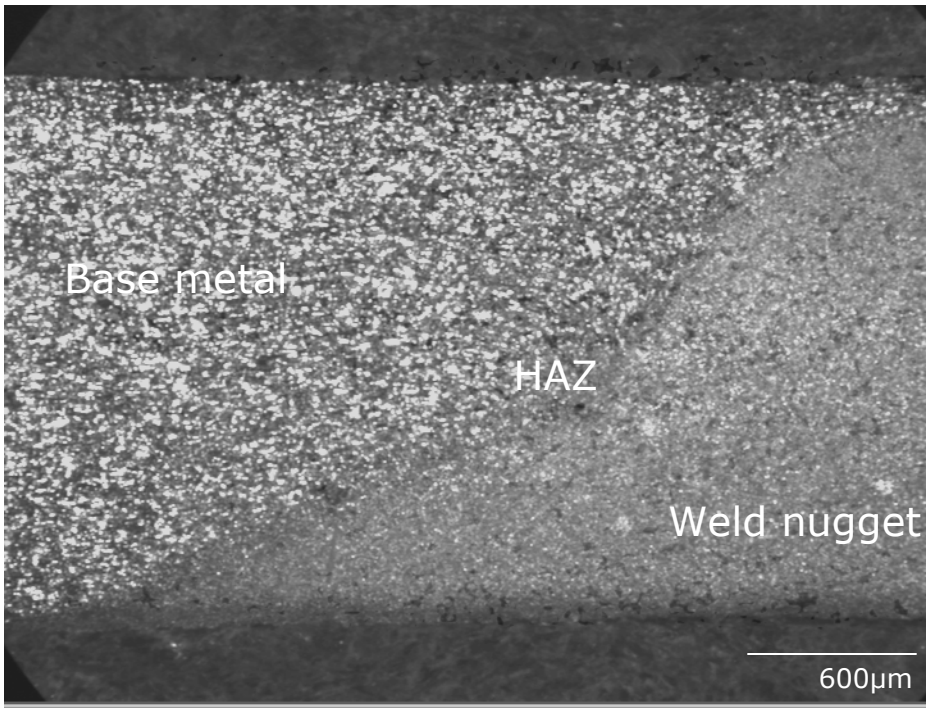

Figure 3-19 Optical microscope image at 5X magnification of AA 7075–T6 showing the base metal, HAZ and weld zone

and the average grain size is measured as 4 µm. Figure 3-21 shows the precipitate of $MgZn_2$ in the interior dendrite arms. Figure 3-22 shows the void of about 300 µm

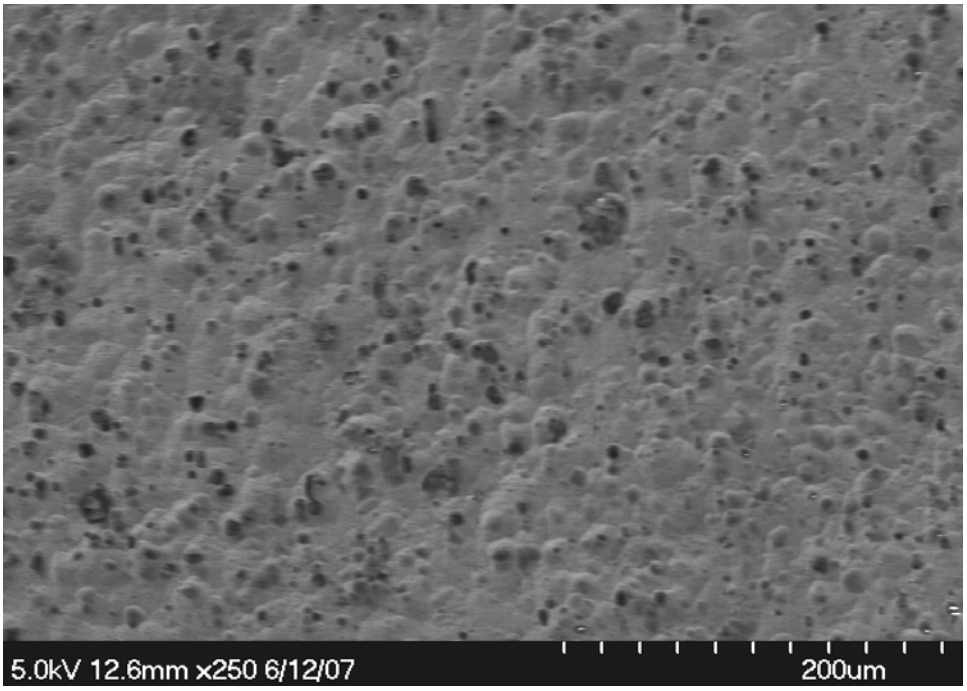

Figure 3-20 Scanning electron microscope image of AA 7075-T6 indicating the grain size in the weld nugget to be ~4µm.

formed in the weld nugget but it can be seen that there is very less effect of this void on the tensile strength of the joint and it is the only void spotted in the weld area.

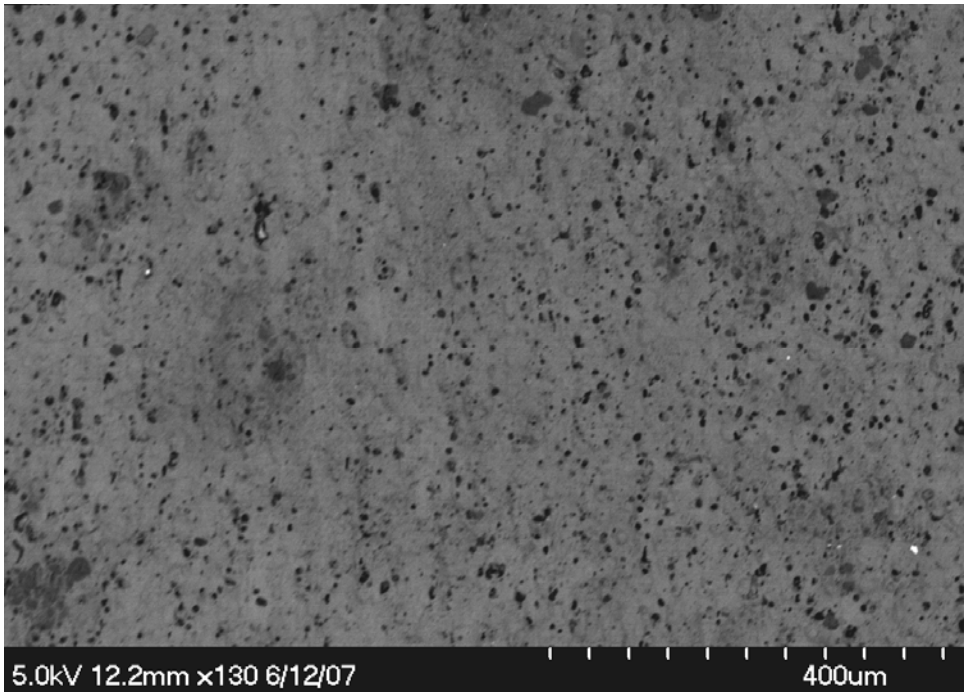

Figure 3-21 Scanning electron microscope image showing the $MgZn_2$ precipitation

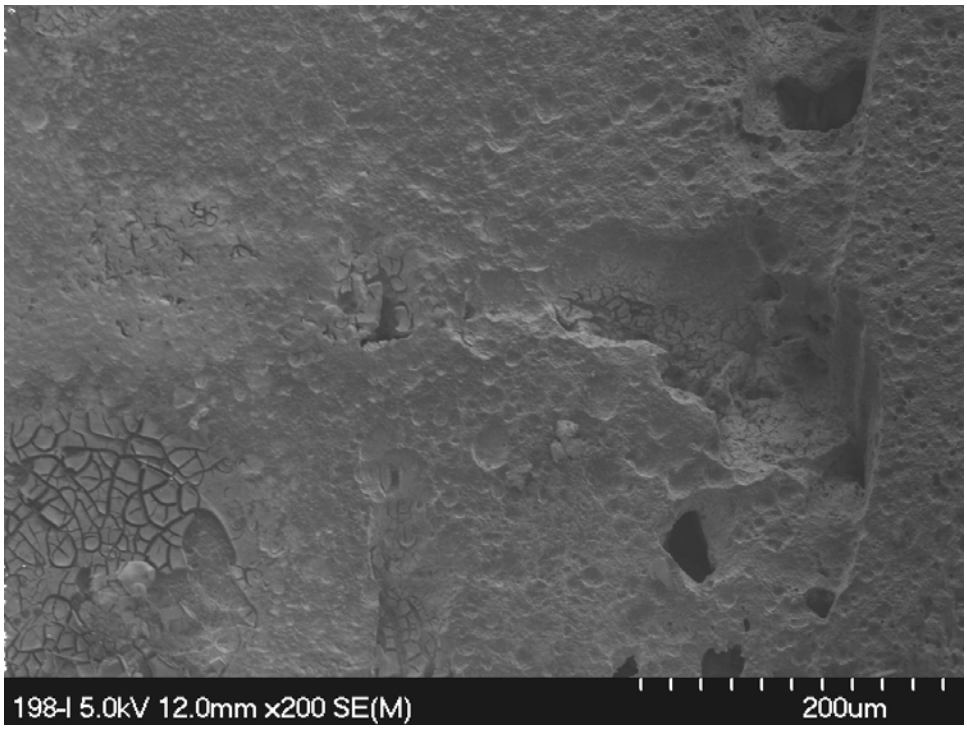

Figure 3-22 Scanning electron microscope image showing the void of ~300μm

The EDS analysis of three different points on the AA 7075–T6 welded sample is analyzed for chemical composition and the three different spots are shown in the Figure 3-23. The first spot is analyzed and the first graph in Figure 3-24 shows that the point 1 in Figure 3-23 is almost pure aluminum and has C, O, F, Cu and Mg in small quantities.

The point 2 of Figure 3-23 is a black spot which has been analyzed by the EDS as carbon reminiscent of carbon formed during the etching process as a result of reaction between the metal and the hydrochloric acids, hydrofluoric acid and nitric acid used in the Keller's etchant. Small quantities of Al, O, Cu and Si are present at the black spot oxygen could be as a result of the reaction between the metal and acid and Al, Cu and Si are the components present in AA 7075-T6.

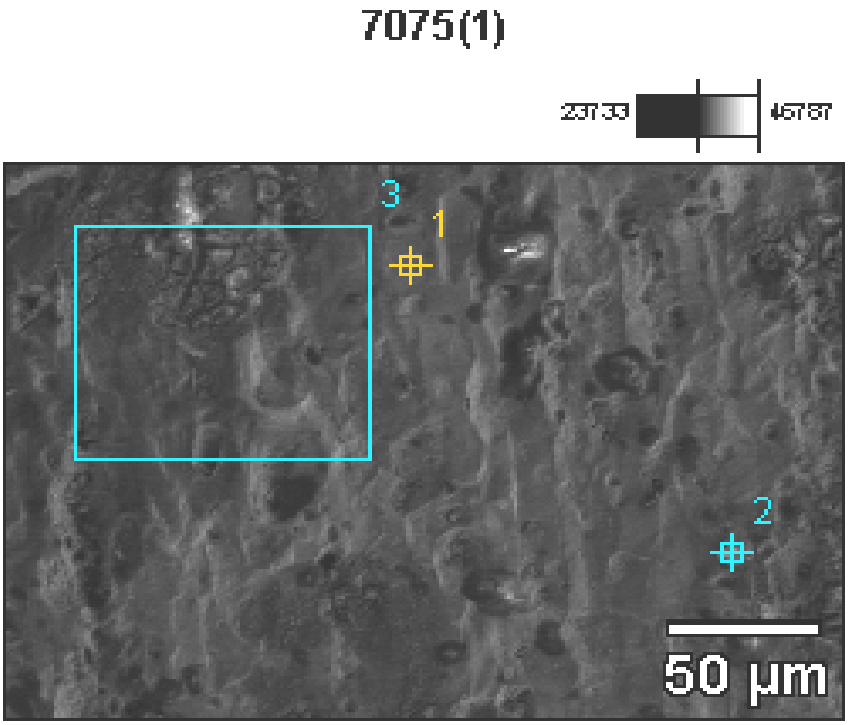

Figure 3-23 Energy dispersive spectrograph figure for analysis of AA 7075–T6 welded sample

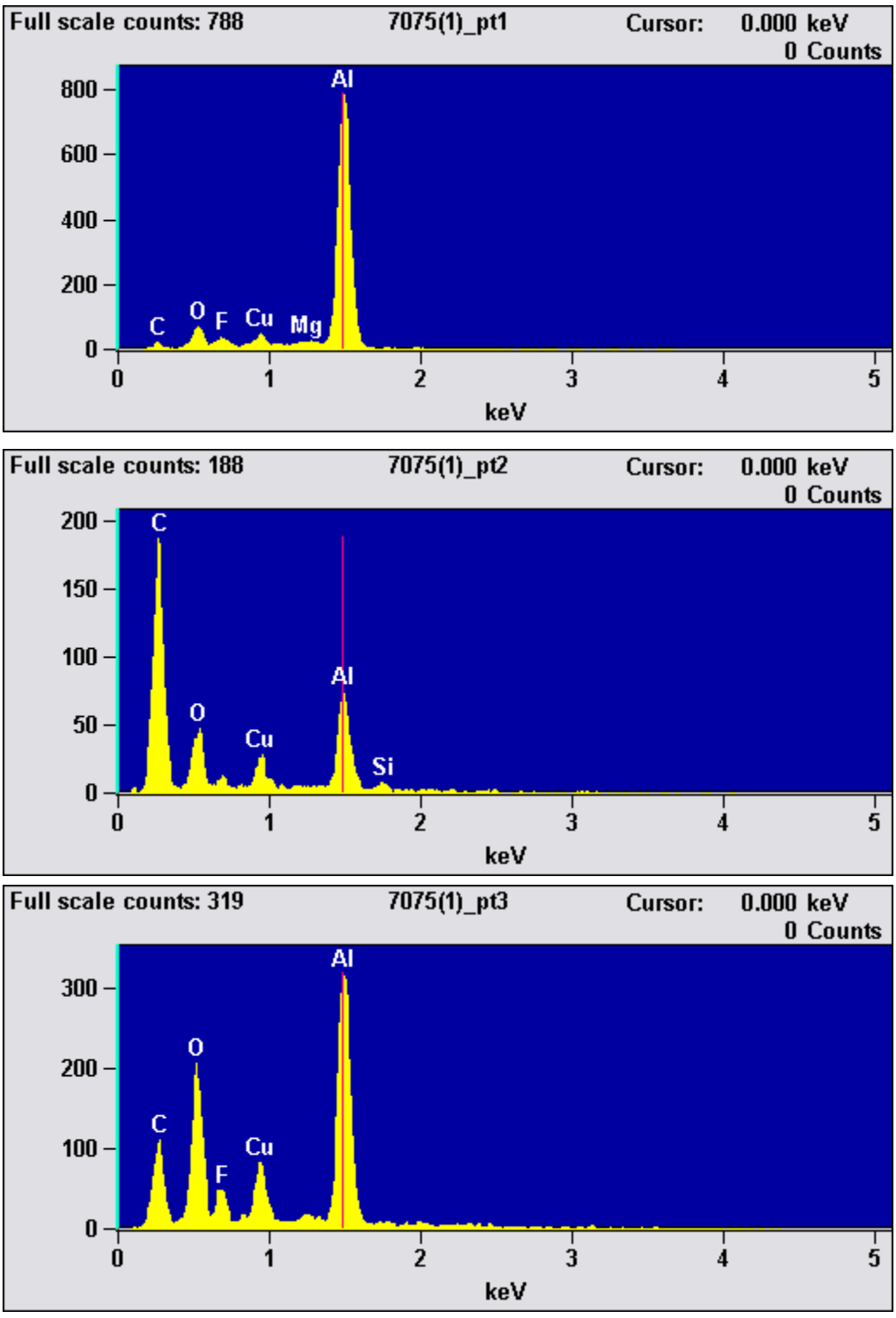

Figure 3-24 Energy dispersive spectrograph analysis of AA 7075–T6 welded sample

The third spot analyzed is bulk analysis done to analyze the composition of the AA 7075-T6, the graph shows that the area 3 in Figure 3-23 has Al, Cu, F, O and C as shown in the third graph of the Figure 3-24.

The study of fractured tensile specimens of friction stir welded AA 7075-T6 is done by analyzing the fractured coupons under the scanning electron microscope. Figure 3-25 and Figure 3-26 show the fractured surface of the tensile samples of AA 7075-T6, Figure 3-25 shows the overall morphology of the sample at very low magnification and it can be seen that the material has not yielded or elongated before the fracture occurred. The crack started on the advancing side and has progressed to the retreating side as the stresses in the advancing side are very high compared to the stress in the retreating side.

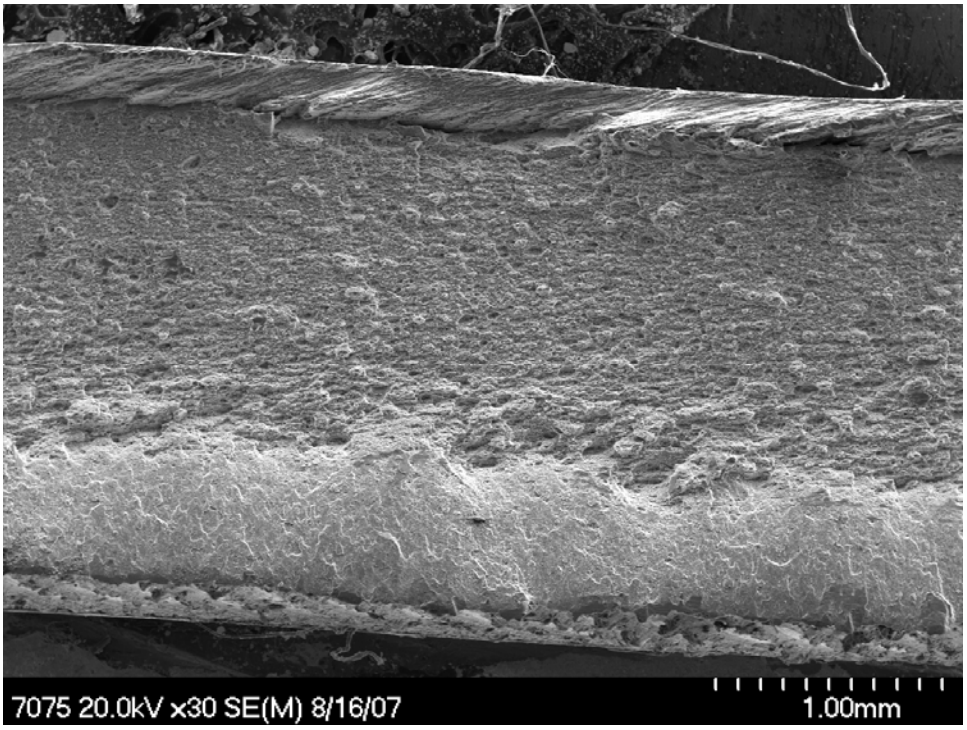

Figure 3-25 Scanning electron microscope image showing the overall morphology of fractured friction stir welded AA 7075-T6 tensile sample

The Figure 3-26 shows the fractured surface at higher magnification of 250X, it can be observed that there is no elongation of the walls of the microscopic dimples and there is no wall formation which is common in the ductile failure. Thus it can be concluded that the specimen has failed due to brittle fracture and lack of ductility.

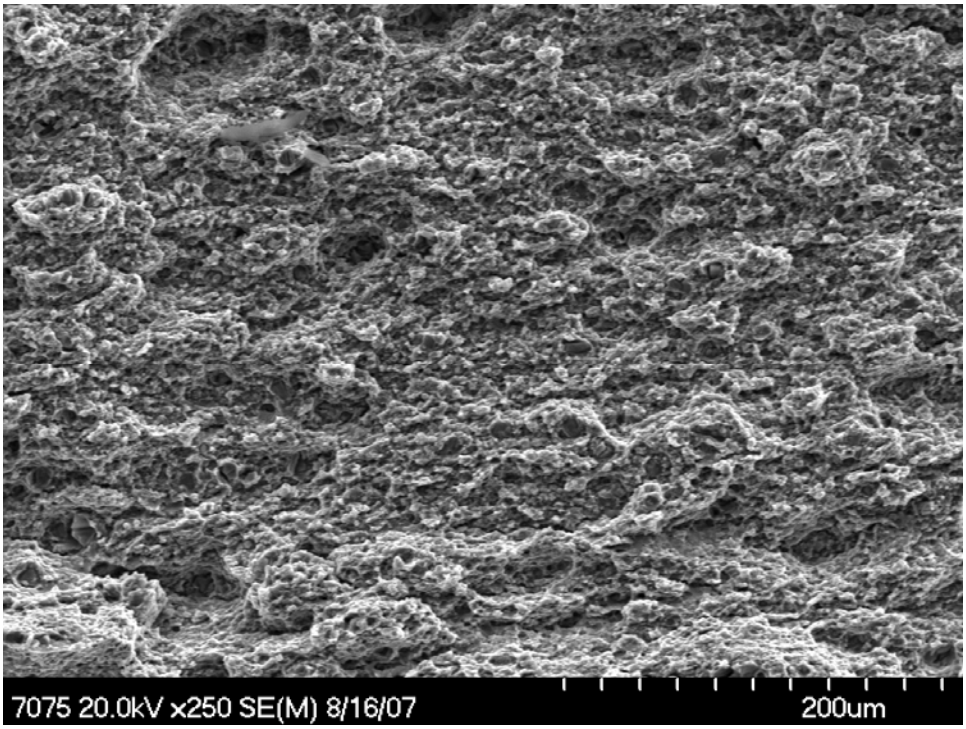

Figure 3-26 Scanning electron microscope image reveals the brittle fracture in the AA 7075-T6 coupon

3.2 Welding of Dissimilar Alloys of Aluminum

The process parameters for the welding of AA 2024-T3 and AA 7075-T6 is decided based on the weld process parameters which has resulted a good weld for the alloys AA 2024-T3 and AA 7075-T6 separately.

Sample number	Spindle speed (rpm)	Feed (in/min)	Plunge depth (in)
Bi – A 1	675	3.625	0.080
Bi – A 2	675	5.75	0.080
Bi – A 3	675	7.625	0.080
Bi – A 4	840	3.625	0.080
Bi – A 5	840	5.75	0.080
Bi – A 6	840	7.625	0.080
Bi – A 7	1045	3.625	0.080
Bi – A 8	1045	5.75	0.080
Bi – A 9	1045	7.625	0.080

Table 3-8 L9 array for the welding of dissimilar aluminum alloys showing the combinations of different process parameters used to fabricate welds.

It is discussed in the previous section 3.1 that the combination of 1045 rpm, 5.75 in/min feed rate and 0.080 in of plunge depth has resulted in a good weld in AA 2024-T3 and a combination of 840 rpm, 7.625 in/min feed rate and 0.080 in of plunge depth has resulted in a good weld in AA 7075-T6. The L9 array for design of experiments to weld dissimilar alloys is given in Table 3-8. Tensile tests and the stretch forming experiments are conducted on the welds fabricated and the results of the tensile test are as shown in Table 3-9.

Sample number	Yield Strength (MPa)	Ultimate Tensile Strength (MPa)	Percent elongation (mm)
Bi – A 1	320	395	26.60
Bi – A 2	325	416	27.80
Bi – A 3	335	355	27.60
Bi – A 4	--	--	--
Bi – A 5	335	354	26.60
Bi – A 6	335	360	28.00
Bi – A 7	317	351	27.00
Bi – A 8	335	364	27.30
Bi – A 9	345	355	26.80

Table 3-9 Results of the tensile test on welded dissimilar alloy joints indicating the yield strength (MPa), ultimate tensile strength (MPa) and percent elongation

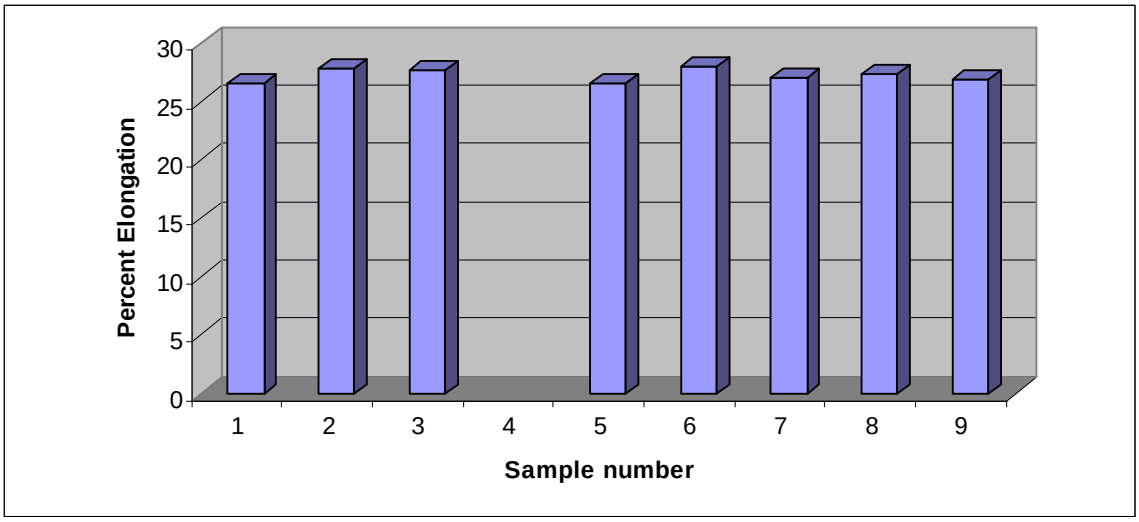

Figure 3-27 Column graph displaying the percent elongation of the samples fabricated from the L9 array for the dissimilar alloys AA 2024-T3 and 7075-T6

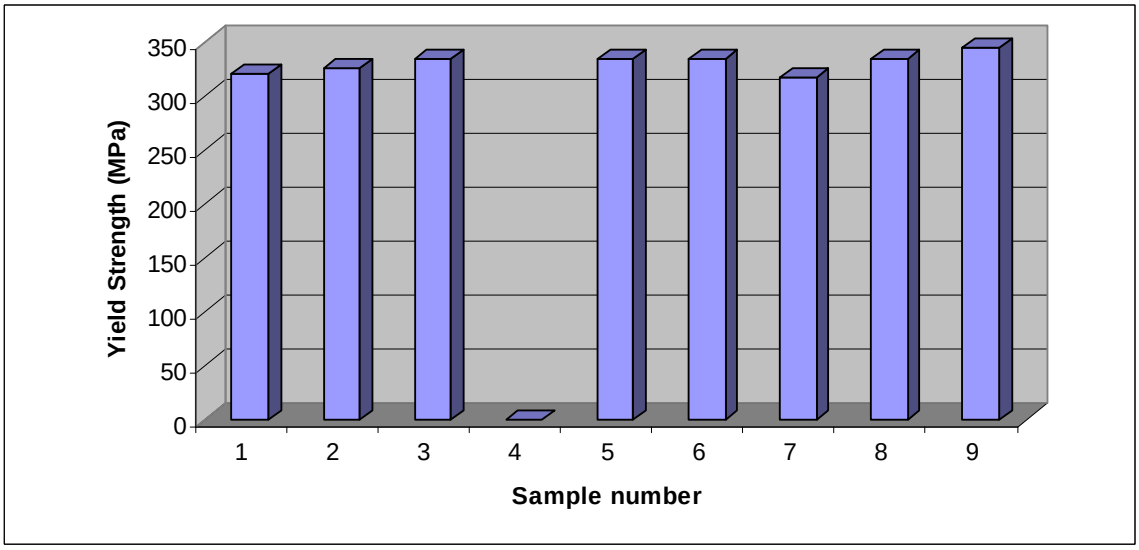

Figure 3-28 Column graph displaying the yield strength (MPa) of the samples fabricated from the L9 array for the dissimilar alloys AA 2024-T3 and 7075-T6

The above graphs compare the percent elongation and the yield strength (MPa) of all the nine samples with each other which are fabricated using the L9 array for the dissimilar alloys AA 2024-T3 and AA 7075-T6.

It can be observed that a combination of 675 rpm 5.75 in/min feed rate and plunge depth of 0.080in has resulted in a good weld which has the highest ultimate tensile strength and a combination of 840 rpm, 3.625 in/min feed rate and plunge depth of 0.080 in has not resulted in the formation of a weld.

The stress – strain curves of the best and the bad welds have been super imposed form the results of the tensile test as shown in Figure 3-29, the area under the stress – strain curve is a representation of the strain energy the tensile sample can take before fracture.

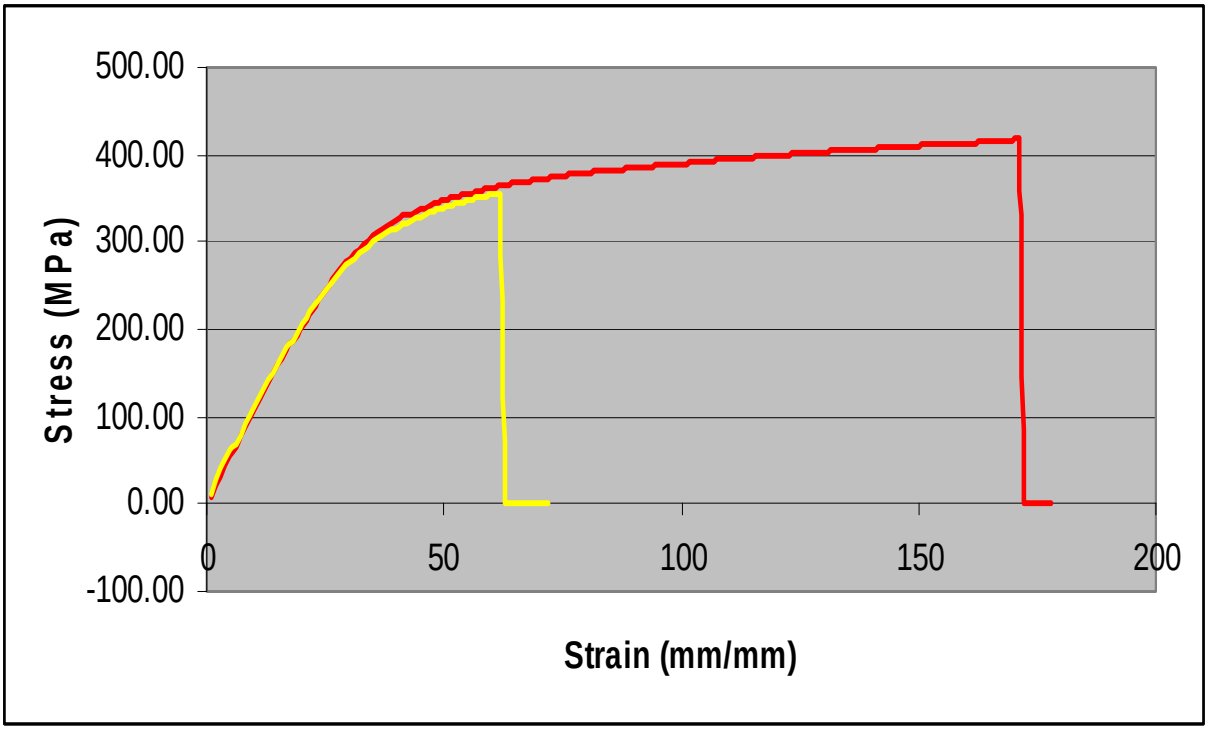

Figure 3-29 Stress – strain curves of the good sample and bad sample of the samples fabricated from AA 2024-T3 and AA 7075–T6 super imposed to compare the toughness of the samples.

The stretch forming is also conducted on the welds fabricated from different alloys on each side. The results of stretch forming also fortify the tensile test results the weld fabricated with a of combination of 675 rpm 5.75 in/min feed rate and plunge depth of 0.080 in as process parameters has formed the most and has a formed depth of 0.95 in. The results of the stretch forming are listed in the Table 3-10.

Sample number	Depth of formed sample (in)
Bi – A 1	0.58
Bi – A 2	0.95
Bi – A 3	0.54
Bi – A 4	--
Bi – A 5	0.65
Bi – A 6	0.73
Bi – A 7	0.45
Bi – A 8	0.48
Bi – A 9	0.55

Table 3-10 listed results of the stretch forming experiments of welds fabricated from dissimilar alloys.

The micro hardness measured from these welds show that the microhardness is higher on the AA 7075-T6 side and lower on the AA 2024-T3 side. The microhardness varies from 165 H_v to 175 H_v in the base metal on AA 7075-T6, HAZ on the AA 7075-T6 side varies from 155 H_v to 165 H_v and the weld nugget varies between 135 H_v to 150 H_v, the HAZ on the AA 2024-T3 side has the least hardness around 100 H_v, the base metal of 2024-T3 has a micro hardness 130 H_v to 135 H_v. Figure 3-30 shows the changes in the micro hardness weld from AA 7075-T6 to AA 2024-T3.

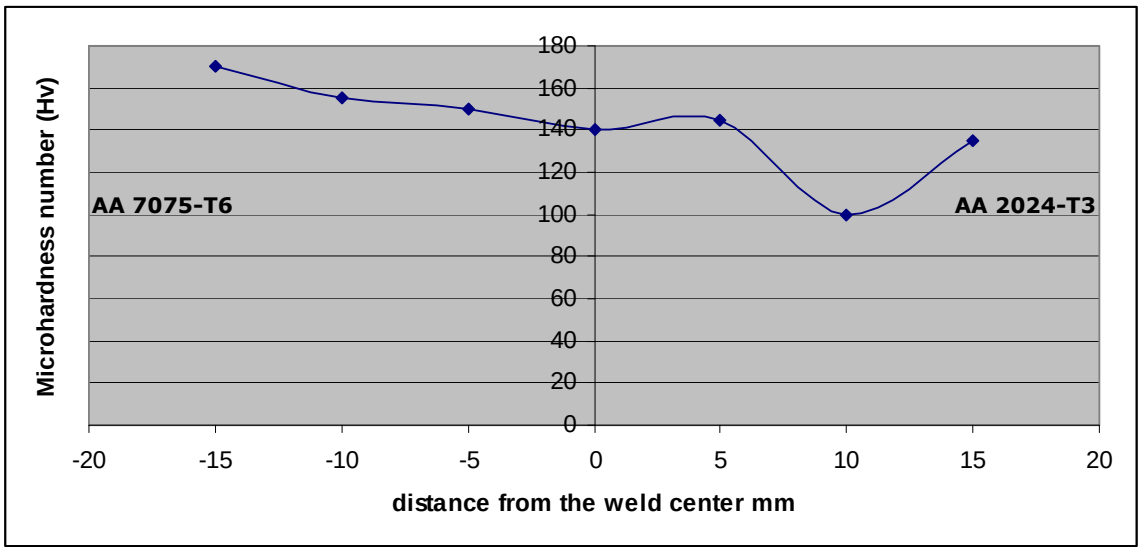

Figure 3-30 Microhardness measure in the joint of friction stir welded AA 2024-T3 and AA 7075-T6, AA 7075 on the left side of weld center.

Figure 3-31 shows a scanning electron microscope image in which there are no defects and the marks on the advancing side can be seen clearly at this magnification but there are no marks on the retreating side of the weld which indicates that the material on the retreating side is under less stressed conditions compared to the material on the advancing side of the weld. The welds fabricated with different process parameters which have yielded low ultimate tensile strength also did not have any external porosity or voids, but there were some internal voids.

Many charged particles were spotted on the surface of the specimens and can be seen at higher magnification.

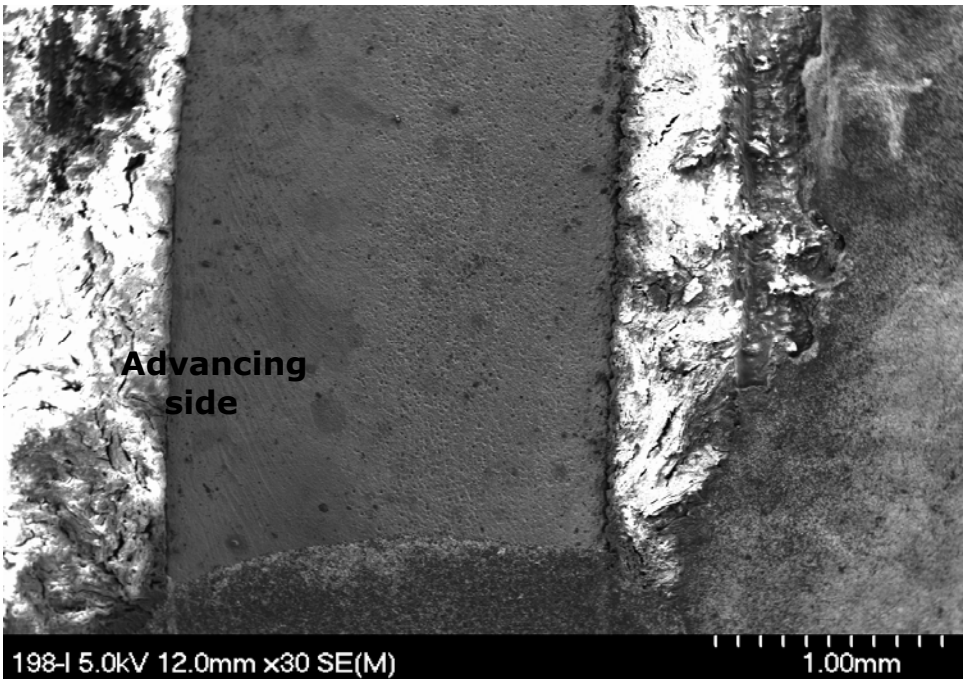

Figure 3-31 Scanning electron microscope image of friction stir welded joint of AA 2024-T3 and AA 7075-T6 which shows the lines on the advancing side

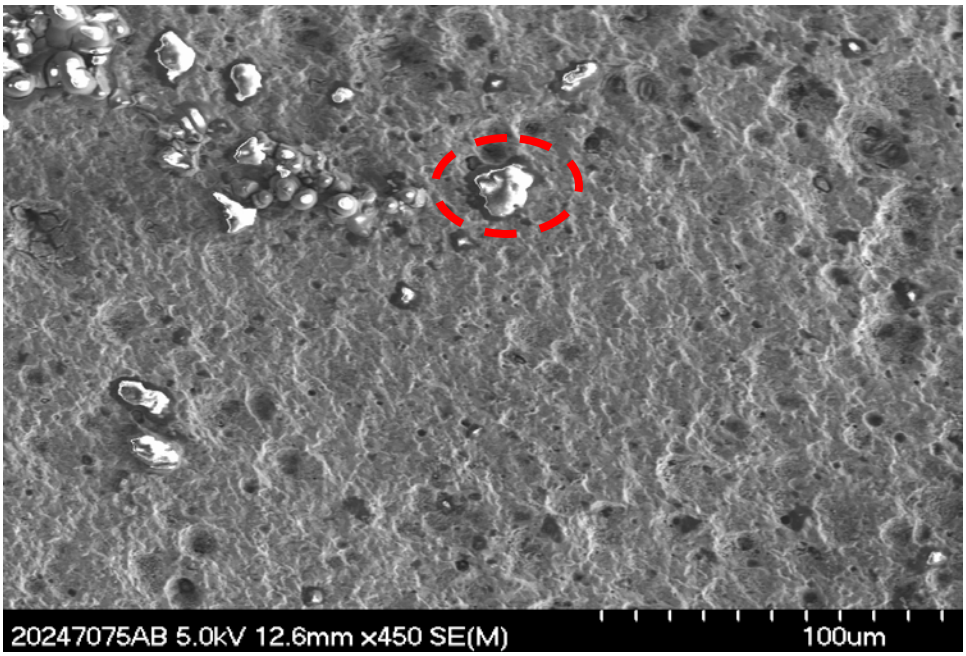

Figure 3-32 Scanning electron microscope image at higher magnification showing the charged particles (carbon) on the etched surface of the AA 2024-T3 and AA 7075-T6 joint.

Figure 3-32 indicates the charged particles on the surface of the sample. Energy dispersive spectroscopy (EDS) analysis has shown that the charged particles on the surface are carbon reminiscent from the reaction of the metal and the acids during the etching process of the samples to reveal the microstructures.

The carbon particles are bright due to the deposition of electrons from the electron gun of the scanning electron microscope, as the carbon particles are insulators the electrons do not have a circuit to escape and the deposition of electrons make the insulating spots look bright. The bright spots were identified as carbon from the EDS analysis. Figure 3-33 is the graph result of the EDS analysis. It can be observed that the bright spot has a major composition of carbon and has oxygen and aluminum in little quantities.

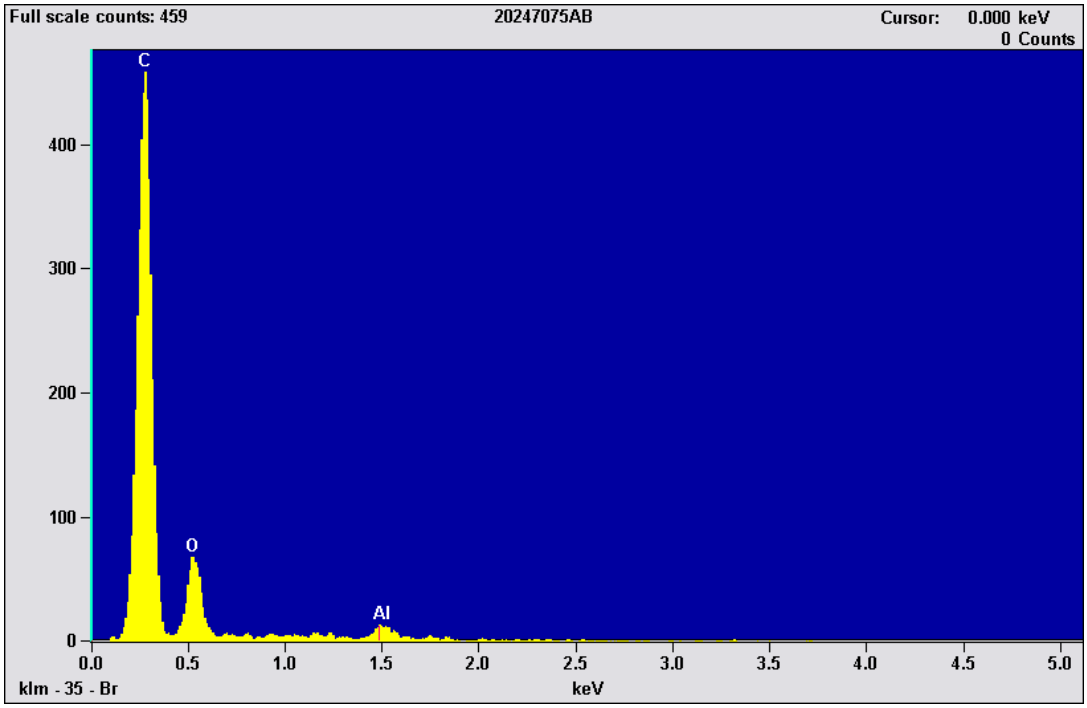

Figure 3-33 Energy dispersive spectroscopy result of the analysis of the bright charged particles on the surface of the etched AA 2024-T3 and AA 7075-T6 joint.

Spot and bulk analysis of some selected points was done to find out the chemical composition and the uniformity of distribution in the metal. Two spots and two circular areas were selected for the analysis as shown in the Figure 3-34. The spot and the bulk analysis results are shown in the four graphs in Figure 3-35.

The analysis revealed the chemicals that are present in the alloys AA 2024-T3 and AA 7075–T6. The chemicals such as C, O, and F are not from the composition of the alloy, C and O are reminiscent from the reaction of the metal and acid reaction during the process of etching, presence of F could be from the hydrofluoric acid used in the preparation of the Keller's etchant used for the etching process of the mounted samples.

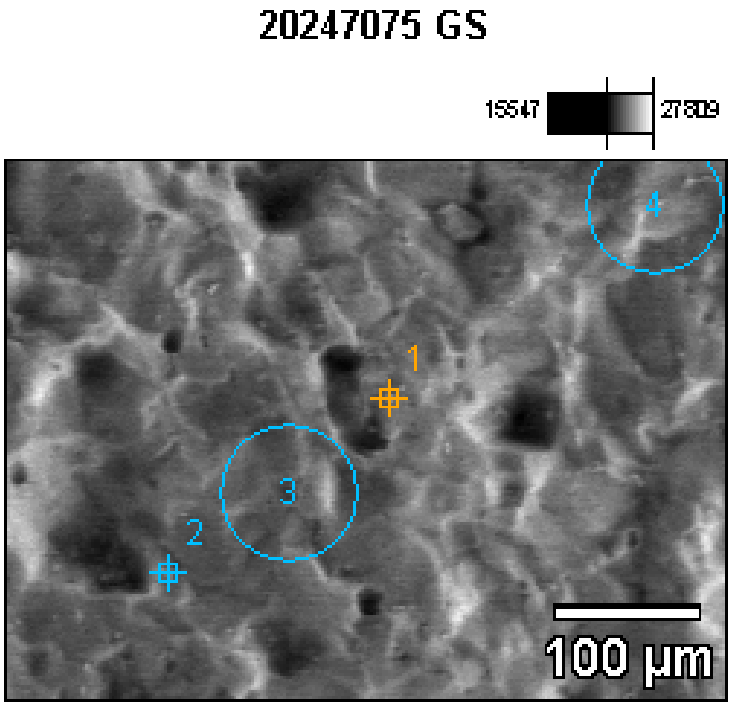

Figure 3-34 Image of the AA 2024-T3 and AA 7075-T6 joint taken under scanning electron microscope and analyzed with the energy dispersive spectroscope.

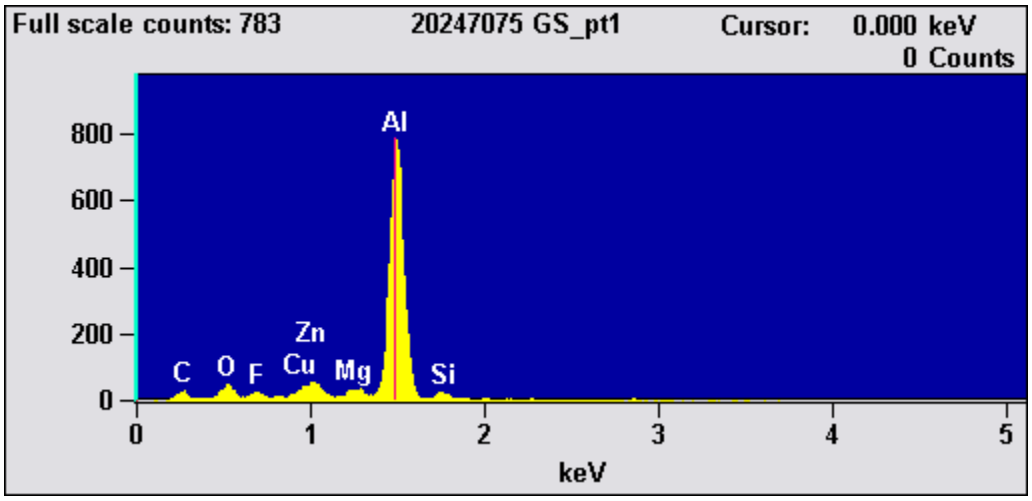
Full scale counts: 783
20247075 GS_pt1
Cursor: 0.000 keV
0 Counts
800
600
400
200
0
Al
Zn
C
O
F
Cu
Mg
Si
0
1
2
3
4
5
keV

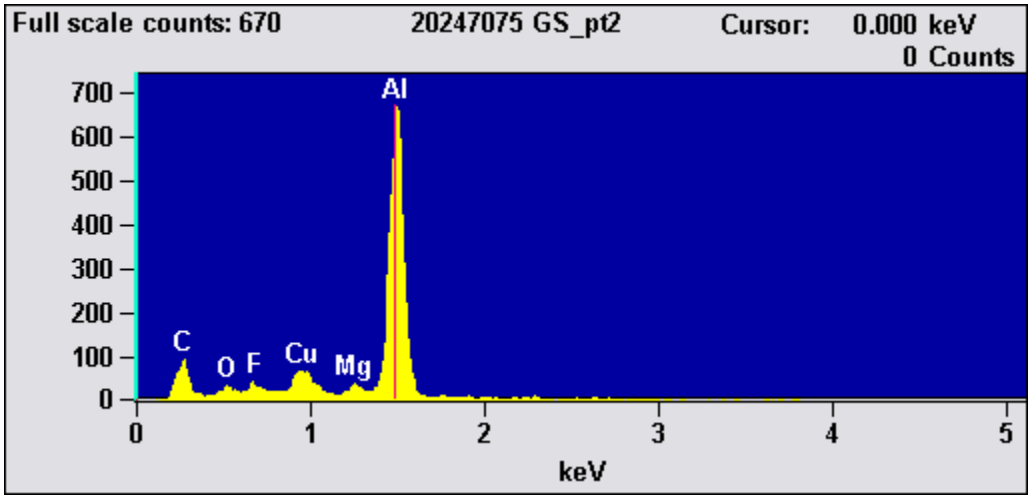
Full scale counts: 670
20247075 GS_pt2
Cursor: 0.000 keV
0 Counts
700
600
500
400
300
200
100
0
Al
C
O
F
Cu
Mg
0
1
2
3
4
5
keV

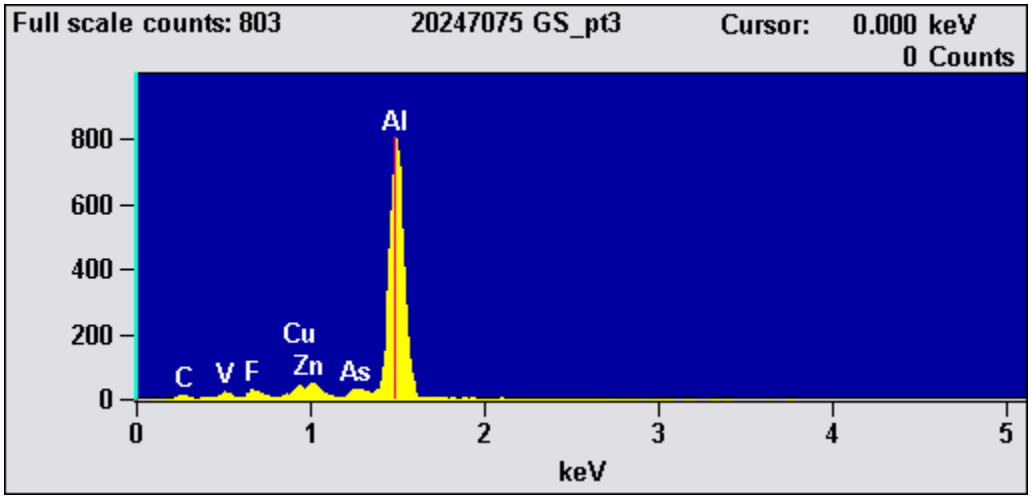
Full scale counts: 803
20247075 GS_pt3
Cursor: 0.000 keV
0 Counts
800
600
400
200
0
Al
Cu
C
V
F
Zn
As
0
1
2
3
4
5
keV

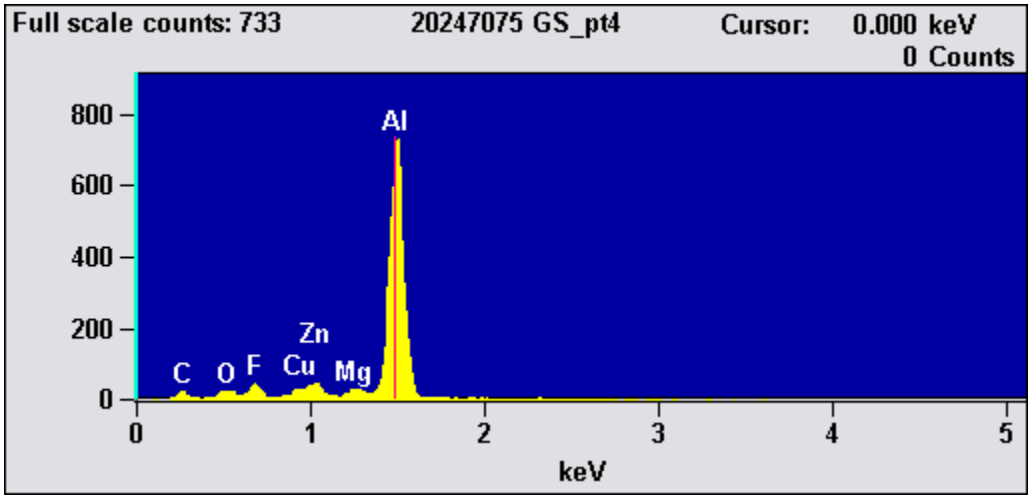

Figure 3-35 Result of Energy dispersive spectroscopy analysis four different spots of joint of AA 2024-T3 and AA 7075–T6 for the chemical composition of the weld

CHAPTER 4: CONCLUSION AND FUTUREWORK

The objective of this research which is to characterize the mechanical properties and studying the microstructures of the friction stir welded alloys fabricated of similar and dissimilar alloys of Al was successfully achieved. The optimal conditions for obtaining a good welded joint is a rotational speed of 1045 rpm, feed rate of 5.75 in/min and a plunge depth of 0.080 in. for AA 2024-T3, rotational speed of 840 rpm, feed rate of 7.625 in/min and a plunge depth of 0.080 in. for AA 7075-T6 and rotational speed of 675 rpm, feed rate of 5.75 in/min and a plunge depth of 0.080 in. for the joining of the dissimilar alloys of aluminum of AA 2024-T3 and 7075-T6.

The mechanical property which reflects the formability of the friction stir welded joints is recognized as ductility, Formability of FSW sheets as measured by ductility in tension test and stretch forming test is acceptable for further processing.

The research could be taken further by applying the same technique to other Aluminum alloys such as 5XXX and 7XXX which are the basic alloys used in the automotive industry. This could help the increase of use of the friction stir welding in the automotive industry. Different design of the tool could be used to investigate the effect of the tool design. The probe shape could be a triangle, square or rectangular one as the probe used for the current research was a cylindrical one with threads on it. The study could be extended to lap joints and investigated the same way.

REFERENCES

1. D. Scott MacKenzie and George E. Totten, 2006, "Analytical characterization of Aluminum, Steel and Superalloys", Atlas of Aluminum microstructures, Chapter 2, PP 55-156.

2. Laurent D'Alvise,2007, "Friction Welding Processes", page number 5

3. M.J. Jones, P. Heurtier, C. Desrayaud, F. Montheillet, D. Allehaux, J.H. Driver, 2005, "Correlation between microstructure and microhardness in a friction stir welded 2024 aluminum alloy", Scripta Materialia, Vol. 52, pp. 693-697.

4. C.G. Rhodes, M.W. Mahoney, W.H. Bingel, R.A. Spurling and C.6. Bampton, 1997,"Effects of friction stir welding on microstructure of 7075 aluminum", Scripta Materialia, Vol. 36, pp. 69-75.

5. Michael A. Sutton, Bangcheng Yang, Anthony P. Reynolds, Junhui Yan, 2004, "Banded microstructure in 2024-T351 and 2524-T351 aluminum friction stir welds Part II. Mechanical characterization", Materials Science and Engineering, Vol. A364, pp. 66-74.

6. P. Cavaliere, R. Nobile, F.W. Panella, A. Squillace, 2006, "Mechanical and microstructural behaviour of 2024–7075 aluminium alloy sheets joined by friction stir welding", International Journal of Machine Tools & Manufacture, Vol. 46, pp. 588-594.

7. Ying li, L.E. Murr and J.C. Mcclure, 1999, "Solid-state flow visualization in the friction stir welding of 2024 al to 6061 Al", Scripta Materialia, Vol. 40, No 9, pp. 1041-1046.

8. M. Cabibbo, H.J. McQueen, E. Evangelista, S. Spigarelli, M.Di Paola, A. Falchero, 2007, "Microstructure and mechanical property studies of AA6056 friction stir welded plate", Materials Science and Engineering, article in press.

9. William D. Lockwood, Borislav Tomaz, A.P. Reynolds, 2002, "Mechanical response of friction stir welded AA2024: experiment and modeling", Materials Science and Engineering, Vol. 323, 348-353.

10. H.J. Liu, H. Fujii, M. Maeda, K. Nogi, 2003, "Tensile properties and fracture locations of friction-stir-welded joints of 2017-T351 aluminum alloy", Journal of Materials Processing Technology, Vol. 142, pp. 692-696.

11. S. Benavides, Y. Li, L.E. Murr, D. Brown, and J.C. McClure, 1999, "Low-temperature friction-stir welding of 2024 aluminum", Scripta Materialia, Vol. 41, No. 8, pp. 809-815.

12. Hua-Bin Chen, Keng Yan, Tao Lin, Shan-Ben Chen, Cheng-Yu Jiang, Yong Zhao, 2006, "The investigation of typical welding defects for 5456 aluminum alloy friction stir welds", Materials Science and Engineering, Vol. A433, pp. 64-69.

13. Box, G. E. P. and Wilson, K.B. (1951) On the Experimental Attainment of Optimum Conditions (with discussion). Journal of the Royal Statistical Society Series B 13(1):1-45.

14. A. Squillace, A. De Fenzo, G. Giorleo, F. Bellucci, 2004, "A comparison between FSW and TIG welding techniques: modifications of microstructure and pitting corrosion resistance in AA 2024-T3 butt joints", Journal of Materials Processing Technology, Vol. 152, pp. 97-105.

15. W. M. ThomasU, E. D. Nicholas, 1997, "Friction stir welding for the transportation industries", Materials & Design, Vol. 18, No. 4/6, pp. 269-273.

16. T. Minton, D.J. Mynors, 2006, "Utilisation of engineering workshop equipment for friction stir welding", Journal of Materials Processing Technology, Vol. 177, pp. 336-339.

17. P. Cavaliere, E. Cerri, A. Squillace, 2005, "Mechanical response of 2024-7075 aluminium alloys joined by Friction Stir Welding", Journal of Materials Science, Vol. 40, pp. 3669-3676.